Coherent phenomena in electron transportthrough a molecular conductor

A. Zazunov

Mémoire pour l'obtention de
l'Habilitation à Diriger des Recherches
présenté par

Alex ZAZUNOV

à l'Université de la Méditerranée
Aix-Marseille II

Spécialité: Physique

Coherent phenomena in electron transport through a molecular conductor

---

Composition du Jury

Mr.	P. Dumas	(Président du Jury)
Mr.	F. W. J. Hekking	(Rapporteur)
Mr.	T. Martin	(Tuteur)
Mr.	G. Montambaux	(Rapporteur)
Mr.	B. Plaçais	(Rapporteur)

Soutenance prévue le 27 septembre 2007

Ce mémoire a été préparé au sein du
Laboratoire de Physique et de Modélisation des Milieux Condensés

RÉSUMÉ

Dans cette thèse d'habilitation, nous considérons plusieurs aspects du transport à travers une molécule unique, connectée à des bornes de métal normal ou à des bornes supraconductrices. L'emphase à été mise sur la détection des signatures les plus marquantes du transport cohérent à travers les molécules, ainsi que sur la compréhension des problèmes de corrélations (problème à N corps) sur la dynamique de ces systèmes, provenant des degrés de liberté internes (vibrations, spin, etc.) du conducteur et affectant le passage du courant.

En ce qui concerne le transport dans le régime normal à travers une molécule qui vibre (un nanotube de carbone suspendu par ses extrémités), nous avons procédé à une étude détaillée de la conductance différentielle négative (CDN) qui est observée dans ces dispositifs. En supposant des contacts tunnel, tel que les électrons qui s'échappent dans les bornes effectivement perdent leur cohérence de phase (c'est-à-dire à haute température), nous avons dérivé les équations cinétiques dans lesquelles la nature quantique de l'interaction électron-phonon au sein du point quantique moléculaire est prise en compte sans approximations (formation de polaron sur le point quantique moléculaire). Le fait que la conductance différentielle soit positive ou négative dépend de la position du niveau polaronique et de l'occupation des pics satellites associés au nombre d'occupation des phonons, qui sont compris entre la tension de source et de drain des électrodes. La CDN apparaît lorsque deux de ces pics satellites entrent en compétition dans le transport, et constitue une signature des effets hors équilibres associés au vibrations de la molécule. Nous avons clairement montré que pour des couplages tunnels asymétriques (situation qui correspond à la géométrie des expériences sur le domaine), on observe un CDN pour un vaste domaine de paramètres. Nous avons également exploré les effets de navette électronique, ou le déplacement de la molécule entre en compte dans l'Hamiltonien tunnel, qui peuvent être détectés en regardant l'asymétrie des courbes courant tension. Bien que le mécanisme de navette tend à renforcer la CDN, il n'est toutefois pas suffisant pour y donner lieu sans hypothèses sur la valeur relative des couplages tunnels.

Nous avons également étudié le transport dans le régime normal à travers un point quantique moléculaire dans le cas d'un couplage fort aux contacts, mais loin du régime Kondo. En utilisant l'approche hors équilibre des fonctions de Green dans la représentation du polaron, nous sommes allés au delà du régime perturbatif pour calculer la caractéristique courant tension dans le régime de

couplage électron-phonon intermédiaire. Nous avons montré qu'en accroissant le couplage tunnel au contacts, les corrélations associées au nuage de polaron deviennent très importantes à haute température, et donnent lieu à une réduction dramatique de l'élargissement des pics la densité d'états de la molécule. Nous proposons une détection de ces phénomènes par la mesure de la conductance différentielle, tout en variant la température locale de la molécule (nanotube de carbone). On note qu'en présence d'un environnement dissipatif les pic satellites dus aux phonons devraient acquérir un élargissement additionnel. L'inclusion des effets d'amortissement des modes phononiques constituerait une extension de ce travail.

Dans cette thèse, nous avons également abordé le problème du transport cohérent en présence de phonons, dans un système moléculaire connecté à des contacts supraconducteurs. Nous avons calculé le courant DC (partie du courant stationnaire) pour toutes les valeurs de la tension à l'aide de l'approche des fonctions de Green Keldysh, pour une fréquence de vibration arbitraire, mais dans le régime du couplage faible électron-phonon. Nos principaux résultats sont les suivants: i) dans le régime sous le gap $eV < \Delta$, les processus de réflexions multiples d'Andreev (MAR) sont accompagnés de processus d'émission/absorption de phonons et donne lieu à une structure très riche près des valeurs de tension ou le nombre de réflexions d'Andreev changent d'une unité (ces tensions sont appelées les "MAR onsets"). On observe alors un effet pair impair ou le courant est augmenté/diminué suivant la transition de "MAR onset" (entre pair/impair et vice versa). Ces phénomènes trouvent un interprétation physique en comparant avec la théorie de la diffusion de Buttiker-Landauer, adaptée au contacts supraconducteurs, une théorie connue sous le nom d' "échelle de MAR". A l'équilibre $V = 0$, nous avons obtenu des résultats analytiques pour le courant Josephson dans la limite adiabatique ou la fréquence de vibration est faible comparée au gap supraconducteur, qui est interprétée en terme des états liés d'Andreev avec une transparence aux contacts renormalisée par les phonons. Pour le futur, une extension de cette théorie au calcul du bruit (fonction de corrélation courant-courant) est envisagée. Le bruit peut en effet procurer une information supplémentaire sur la charge transmise à travers la jonction, et il serait intéressant d'étudier l'effet des phonons dans ce cadre.

Nous avons également considéré le cas des contacts supraconducteurs, mais cette fois pour les interactions fortes, et uniquement à l'équilibre ou le courant Josephson dépend de la différence de phase entre les deux supraconducteurs. Cette fois on s'intéresse à un diagnostique sur l'état des phonons sur le point quantique moléculaire. Nous trouvons que pour le régime de faible couplage tunnel, des états non-classiques de type "chat de Schrodinger" (une superposition d'états cohérents opposés) sont associés aux états du courant et donc aux liés d'Andreev dans la jonction. Ces états non classiques peuvent être explicités en procédant à une mesure projective du courant. Pour des contacts transparents, nous avons montré que l'effet Josephson génère des fluctuations de phonon

cohérentes, et induit des états quantiques “comprimés” de phonon, analogues aux états “comprimés” de photons en optique quantique: l'impulsion canoniquement conjuguée à la distorsion de la molécule possède des fluctuations inférieures a la valeur minimale habituelle de fluctuations du point zéro. La compression d'états de phonons s'observe pour une grande plage de paramètres: elle est contrlée par la différence de phase et devient maximale près de la transition de polaron. La détection expérimentale de tels états comprimés pourrait être effectuée en nanoélectronique à l'aide de nanotubes suspendus. Il faudrait recourir à un diagnostique optique tel que l'effet Raman résonant, pour démonter l'existence de ces états de phonons non-classiques.

Une autre manière d'explorer les phénomènes cohérents dans le cadre du transport Josephson est d'étudier les situations ou les degrés de liberté de spin des électrons du point quantique moléculaire et des électrodes sont importants. Nous avons donc calculé le courant Josephson à travers un point quantique moléculaire doté d'un grand spin, qui possède une interaction d'échange avec l'électron du point quantique. Ce couplage d'échange peut donner lieu à une transition à l'état pi de la jonction (relation courant phase opposée par rapport a une jonction normale, de phase 0). La contribution relative du courant provenant des états liés d'Andreev et du continuum détermine si la jonction est dans l'état 0 ou l'état pi. Un débouché possible de cette étude est d'étudier les effets de décohérence, et de rétroaction du supercourant sur la dynamique du spin moléculaire.

Dans un autre contexte, les effets de spin associé au courant Josephson ont été étudiés pour un point quantique possédant plusieurs nivaux, et sujet à l'interaction spin orbite Rashba et Dresselhaus. Pour un point quantique ne possédant qu'un seul niveau les effet du couplage spin orbite sont inexistants en l'absence d'un champ magnétique externe. En présence de ce dernier, le courant de ce point quantique possède des oscillations de type Datta Das en fonction du paramètre de couplage spin orbite multiplié par la longueur du point quantique. Ces oscillations ont une amplitude de quelques dixièmes du courant nominal Josephson, et pourraient donc être observées expérimentalement. Le cas d'un point quantique possédant plusieurs niveaux est plus intéressant. Pour un point quantique à deux niveaux en particulier, Le courant possède une dépendance sur le couplage spin orbite même en l'absence de champ magnétique. Le supercourant possède des maxima et des minima marqués pour certaines valeurs de ce couplage. Leur observation constituerait une première évidence du fonctionnement d'un transistor à effet spin orbite dont les bornes sont supraconductrices. Dans le futur il serait intressant d'inclure les interactions Coulombiennes sur le dot.

Nous avons développé en parallèle une théorie pour modéliser un bit quantique basé sur les états liés d'Andreev: un dispositif constitué d'un SQUID (dispositif d'interférométrie supraconducteur) et d'un contact ponctuel supraconducteur, combinant donc un circuit macroscopique et microscopique. Le contact ponctuel - qui implique une transparence elevée entre les contacts, peut être vu comme un point quantique qui contient deux états fermioniques localisés, à leur tout

couplés à la dynamique de la phase supraconductrice (un mode bosonique local). Nous avons étudié la décohérence de ce bit quantique d'Andreev, associée à un couplage des électrons des contacts avec des modes de phonons acoustiques. La nature fermionique des nivaux d'Andreev n'affecte pas le pilotage du bit quantique, mais elle joue un rle important en ce qui concerne sa décohérence: la relaxation et le déphasage induit suivent une loi de puissance dans le temps plutt qu'une exponentielle. De plus, nous avons trouvé que le taux de transition entre les nivaux du bit quantique, induit par les transition phononiques est réduit de manière considérable comparé au taux de transition électron-phonon dans les contacts: l'étalement de la fonction d'onde de ses niveaux dans les contacts réduit l'espace de phase disponible pour ces transitions assistées par les phonons.

Dans une étude séparée, nous nous sommes intéressé à la mesure du bruit à haute fréquence ainsi qu'a celle des moments supérieurs du courant, à l'aide d'un circuit résonant en présence de dissipation. Le circuit résonant est couplé à un circuit mésoscopique placé dans le régime cohérent. L'information sur les moments supérieurs du courant est codée dans les histogrammes de la charge du condensateur du circuit résonant. La dissipation est prise en compte par le modèle de Caldeira Leggett, et il est essentielle de l'inclure pour obtenir des fluctuations de charge (donc un bruit mesuré) finies. Nous identifions également quelle Combinaison des corrélateurs de courant entrent dans l'expression du troisième moment mesuré. Ce dernier fait appel à la même susceptibilité généralisée que pour le bruit mesuré, mais elle ne diverge pas dans la limite d'un circuit non dissipatif. Les prédictions sur la mesure de ces quantités sont testées pour le cas du bruit émanant d'un contact ponctuel.

This thesis is based on the work contained in the following papers referred to by Roman numbers in the main text:

I **Andreev level qubit**
A. Zazunov, V. S. Shumeiko, E. N. Bratus', J. Lantz, and G. Wendin,
Phys. Rev. Lett. **90**, 087003 (2003).

II **Dynamics and phonon–induced decoherence of Andreev level qubit**
A. Zazunov, V. S. Shumeiko, G. Wendin, and E. N. Bratus',
Phys. Rev. B **71**, 214505 (2005).

III **Phonon–mediated negative differential conductance in molecular quantum dots**
A. Zazunov, D. Feinberg, and T. Martin,
Phys. Rev. B **73**, 115405 (2006).

IV **Superconducting transport through a vibrating molecule**
A. Zazunov, R. Egger, C. Mora, and T. Martin,
Phys. Rev. B **73**, 214501 (2006).

V **Phonon squeezing in a superconducting molecular transistor**
A. Zazunov, D. Feinberg, and T. Martin,
Phys. Rev. Lett. **97**, 196801 (2006).

VI **Controllable π junction in a Josephson quantum–dot device with molecular spin**
C. Benjamin, T. Jonckheere, A. Zazunov, and T. Martin,
Eur. Phys. J. B **57**, 279 (2007).

VII **Josephson current through a quantum dot with spin–orbit coupling**
L. Dell'Anna, A. Zazunov, R. Egger, and T. Martin,
Phys. Rev. B **75**, 085305 (2007).

VIII **Transport through a molecular quantum dot in the polaron crossover regime**
A. Zazunov and T. Martin, to appear in Phys. Rev. B (2007).

IX **Detection of finite frequency current moments with a dissipative resonant circuit**
A. Zazunov, M. Creux, E. Paladino, A. Crépieux, and T. Martin,
to appear in Phys. Rev. Lett. (2007).

CONTENTS

CHAPTER 1

INTRODUCTION

This thesis presents the main part of my research that I have been conducting after obtaining the PhD degree in 2002. During the past four years, my work has primarily been focused on the theoretical studies of quantum transport phenomena in mesoscopic systems like molecular quantum dots and quantum point contacts. To a large extent, these studies have been motivated and inspired by the impressive advance of nanofabrication technologies.

The field of molecular electronics has seen a tremendous expansion in recent years due to the realization of ingenious experimental setups and the achievement of reproducible results and behaviors. The prospect of using molecules as the fundamental building blocks of future nanoelectronics devices is rather innovating and exciting from the point of view of potential applications. An important difference between electronic transport through individual nanoscale objects, such as molecules, short carbon nanotubes, or DNA, and conventional mesoscopic transport through quantum dots or granular islands arises because molecules can have intrinsic dynamical degrees of freedom (phonons, magnetic spin). Thus, on the fundamental side, the field of molecular electronics opens new directions for studying the interplay of electronic transport and bosonic excitations. Connecting molecules (carbon nanotubes) to superconducting leads promises a rich terrain of exploration of interesting fundamental physics in view of persistent macroscopic quantum coherence. Although a significant progress has been made in theory, the agreement with experiments is not always satisfactory. The challenges for a complete understanding of transport through molecular objects are still considerable. This thesis is a modest attempt to face these challenges.

In outline, the plan of the thesis is as follows. In the next chapter we consider transport through a molecular quantum dot (suspended carbon nanotube) coupled to two normal metallic leads. The molecular dot is modeled as a single resonant level coupled to a local vibrational mode. In the regime of weak tunneling coupling, we focus on the study of the effect of negative differential conductance associated with phonon-mediated electron tunneling processes. A detailed explanation of this phenomenon is provided in terms of the polaron level sidebands, stressing the role of asymmetry in both the tunneling and capacitive

couplings to the leads. In the strong tunneling limit, we focus on the broadening of the Franck-Condon peaks in the differential conductance due to electron tunneling and discuss the role of correlations between phonon clouds in the polaron crossover regime. Going beyond the existing polaron approaches to molecular transport, we develop a nonperturbative scheme which incorporates the retardation effects of the polaron cloud, and is applied to calculate the electron spectral function of the molecule.

In Chapter 3, electronic transport through a molecular conductor is studied for the case of superconducting leads. For the first time, we develop a theoretical framework to include vibrations into superconducting transport in the most interesting quantum-coherent low temperature regime. For weak electron-phonon coupling, we compute the dc current for the entire bias voltage range and provide a physical interpretation of our results in terms of inelastic multiple Andreev reflection processes. In the case of strong vibronic coupling, particular attention is devoted to the influence of Josephson transport on the dynamics of the local vibrational mode. We analyze the ground-state properties of a superconducting molecular transistor and discuss the generation of nonclassical phonon states by exploiting the coherent regime of polaron dynamics.

In Chapter 4, we study the Josephson transport through a single molecular magnet which is modeled as a quantum dot with a local Zeeman field (large frozen molecular spin). We investigate the effect of the Zeeman coupling on the Josephson current-phase relation and discuss the role of Andreev bound states and the quasiparticle continuum in the transition to a π junction with negative critical current. In this chapter, we also study the effect of Rashba and Dresselhaus spin-orbit couplings on the Josephson current through a multilevel quantum dot in a two-dimensional electron gas, and analyze in detail the simplest cases of a single and of two dot levels.

In Chapter 5, we investigate the dynamics of a two-level Andreev bound state system in a highly transmissive quantum point contact embedded in a superconducting loop and discuss the possibility to employ the Andreev levels for quantum information processing. We provide a full quantum mechanical treatment of the Andreev levels coupled to the quantum fluctuations of the superconducting phase difference which plays the role of a local bosonic mode in the Andreev-level "quantum dot". We also analyze the effect of electron-phonon interaction in the bulk electrodes on the coherent dynamics of Andreev states and estimate the phonon-induced decoherence time of Andreev level qubit.

In Chapter 6, we consider the measurement of higher current moments with a dissipative resonant circuit, which is coupled inductively to a mesoscopic device in the coherent regime. The role of dissipation is shown to be essential for the measured noise to remain finite. We identify which combination of current correlators enters the measurement of the third moment and illustrate this for a quantum point contact.

Finally, in Chapter 7, we summarize the obtained results.

CHAPTER 2

NORMAL ELECTRON TRANSPORT THROUGH A MOLECULAR QUANTUM DOT

2.1 PHONON–MEDIATED NEGATIVE DIFFERENTIAL CONDUCTANCE

Motivation

The interplay between electronic and vibrational degrees of freedom is important for understanding transport properties of single-molecule devices. On the fundamental side, this also provides new opportunities in the study of different conduction mechanisms. Single-wall carbon nanotubes are ideal single molecules because of their long length that allows spatially resolved measurements. When nanotubes are contacted by electrodes they form in most cases contacts with a large resistance, which results in Coulomb blockade behavior. This type of single-electron tunneling devices have also been fabricated with the nanotubes suspended between the two electrodes [1, 2, 3]. For this setup geometry, the interesting possibility occurs that mechanical motion affects electrical current and vice versa.

A recent work [1, 2] considered electron injection from a scanning tunneling microscope (STM) tip into a single-wall carbon nanotube freely suspended over a trench (see Fig. 2.1). The STM tip was located near the center of the suspended part of the nanotube. A dc bias voltage V was applied between the substrate and the STM, and the current flowing through the STM-tip - nanotube - substrate structure was measured at a given tunneling distance. In [1, 2], the authors observed additional side peaks near the main Coulomb peaks, which were attributed to phonon-assisted tunneling due to exciting the radial breathing mode (RBM) in the suspended portion of the nanotube. Interestingly, the authors mention frequent detection of negative differential conductance (NDC) regions. Striking NDC features also appear in a very recent work by Sapmaz *et al.* [3], in a transport measurement of a suspended nanotube. In [3], phonon side peaks are attributed to longitudinal stretching modes, and the steps in the current-voltage characteristics are followed by spikes, thus displaying NDC features.

The purpose of paper III is to show that such NDC features can be described

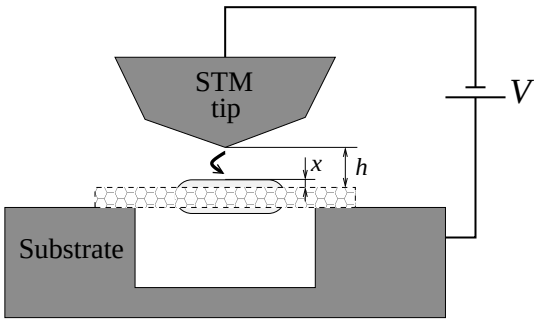

Figure 2.1: Schematic drawing of a carbon nanotube suspended over a trench. A bias voltage is applied between the STM tip (source) and substrate (drain). The inflated portion in the suspended portion of the nanotube illustrates the radial breathing mode. h is the tip–nanotube separation at rest.

within a generic model of a single electron level coupled to two leads and to a local vibration (phonon) mode. Due to the strong electron-phonon interaction (which is the case in [1, 3]), the physics of NDC appears to be a consequence of the transport through the small-polaron states on the molecule. A peculiarity of the system considered in Ref. [1] is that the tunneling couplings of the nanotube to the STM tip and to the substrate are highly asymmetrical. We show that given this asymmetry, NDC behavior can be obtained for a wide range of parameters. Our approach for the description of NDC is by no means restricted to the experimental geometry of Ref. [1], which can be considered as an "experimental paradigm" for phonon-assisted molecular transport.

Theoretical model and rate equation approach

We model a suspended carbon nanotube as a molecular quantum dot which is weakly coupled to two metallic electrodes by tunnel junctions. In the STM geometry (see Fig. 2.1), the leads represent the STM tip and substrate, to which we refer as the "left" (L) and "right" (R) electrodes, respectively. Each tunnel junction ($j = L, R$) is characterized by a resistance (R_j) and a capacitance (C_j). We focus on the strong Coulomb blockade regime, assuming that the number of electrons which can be added to the dot is restricted to 1. The extra-charge electron state is linearly coupled (with the coupling energy g) to a local phonon mode (of frequency Ω) associated with the RBM in [1, 2]. The model Hamiltonian then reads (spin degrees of freedom are neglected, and we use $\hbar = 1$):

$$H = (\epsilon - gx)\, d^\dagger d + \Omega\, b^\dagger b + H_T + H_{leads}\ , \tag{2.1}$$

where the operator d ($d^\dagger$) annihilates (creates) an electron on the dot level of energy ϵ, the bosonic excitations are annihilated (created) by b ($b^\dagger$), and $x = b + b^\dagger$. The leads are described by non-interacting electrons with a constant density of

states, and the tunneling Hamiltonian is given by

$$H_T = \sum_{jk} \mathcal{T}_j \, c_{jk}^\dagger \, d + h.c. \ , \tag{2.2}$$

where c_{jk} ($c_{jk}^\dagger$) annihilates (creates) an electron with momentum k in lead j, and $\mathcal{T}_j$ is a tunneling matrix element which is assumed to be energy-independent.

In the Hamiltonian (2.1), the charging effects are taken into account via the bias-voltage dependence of the position of the dot level ϵ with respect to the chemical potentials of the leads, μ_j. In our approach, ϵ includes the change in the charging energy of the dot when an extra electron is added to the dot and which is obtained from the electrostatic energy consideration:

$$\epsilon - \epsilon_0 = 2E_C(n_x + 1/2) + e\phi \ , \tag{2.3}$$

where ϵ_0 is the "bare" energy level in the dot, $E_C = e^2/2C$ is the charging energy, $C = C_L + C_R$, en_x is a background (fractional) charge, and the potential ϕ of the dot is given by

$$\phi = \sum_j c_j \mu_j / e \ , \quad c_j = C_j / C \ . \tag{2.4}$$

Experimentally, the addition of voltage gates on a molecular transport setup is still challenging but it is possible to achieve in a nanometer-scale region [4, 2]. Yet there is also a motivation to study a setup where the molecular levels are "floating" instead of being fixed by a gate. Besides the strong asymmetry of the tunneling rates, a specific feature of our work is that NDC can occur in such absence of gate voltage, and that the ratio of the capacitance ratio C_L/C_R plays an important role, as it dictates the location of the molecular levels.

In our model, the local vibration is not coupled to any environmental degrees of freedom, like phonon modes or electron-hole excitations in the substrate. Although such coupling is relevant in some experiments, the very high phonon quality factors ($Q > 20000$) obtained in [1] justify to neglect it as a first step.

Assuming weak coupling to the leads, it is advantageous to eliminate the electron-phonon coupling in (2.1) by the unitary transformation $\tilde{H} = U^\dagger H U$, with

$$U = e^{-i\alpha p \, d^\dagger d} \ , \quad p = -i\left(b - b^\dagger\right) \ , \quad \alpha = g/\Omega \ . \tag{2.5}$$

In the rotated basis, the electron state in the dot becomes "dressed" with phonons, forming a small polaron. This results in the "polaron shift" of the dot level energy, $\tilde{\epsilon} = \epsilon - g^2/\Omega$, and a renormalization of the dot-lead tunneling couplings:

$$\tilde{H}_T = \sum_{jk} \mathcal{T}_j \, e^{-i\alpha p} \, c_{jk}^\dagger \, d + h.c. \ . \tag{2.6}$$

Even at relatively high temperatures (a few Kelvins), the dynamics within nano-scaled objects like nanotubes remains phase coherent. On the other hand,

the tunneling rates $\Gamma_{L,R}$ are typically small compared to temperature. This allows us to apply the rate equation approach within the sequential tunneling regime. Based on the assumption that the leads are in thermal equilibrium at given chemical potentials $\mu_{L,R}$, we have derived a kinetic (master) equation for the reduced density matrix of the dot by tracing out the electrode degrees of freedom. The long-time behavior of the reduced density matrix is determined by a set of coupled rate equations for the electron-phonon joint probabilities P_n^i of the dot being in a state with $i = \{0, 1\}$ additional electron and $n = \{0, 1, 2, ...\}$ boson excitation(s). In the steady state, the system of rate equations takes the form:

$$\begin{aligned} \partial_t P_n^0 = 0 &= -\mathbf{\Gamma}_n^< P_n^0 + \textstyle\sum_m \Gamma_{nm}^> P_m^1 \ , \\ \partial_t P_n^1 = 0 &= -\mathbf{\Gamma}_n^> P_n^1 + \textstyle\sum_m \Gamma_{nm}^< P_m^0 \ , \end{aligned} \tag{2.7}$$

with $\mathbf{\Gamma}_n^{>,<} = \sum_m \Gamma_{mn}^{>,<}$. Here $\Gamma_{nm}^{>(<)}$ is the partial transition rate involving hopping an electron from (on) the dot to (from) the leads and changing the phonon occupancy from m to n. The partial rates are determined by the matrix elements between the displaced oscillator states corresponding to the 0 and 1-charge states of the dot, $\gamma_{nm} = \langle n|e^{-i\alpha p}|m\rangle$, and also depend on the Fermi distributions of the leads.

From the solution of Eq. (2.7) we can calculate the dc current and expectation values of the phonon observables expressed in terms of the joint probabilities P_n^i.

Phonon–assisted transport for highly asymmetrical tunneling couplings

In calculating the current-voltage ($I(V)$) characteristics, we focus on the case of highly asymmetric double junction model with $\Gamma_L \ll \Gamma_R$, which corresponds to a typical experimental situation with STM measurements. For instance, in STM measurements on suspended nanotubes, the typical ratio $R_{tip}/R_{sub} \sim 10^3 - 10^5$ can be huge depending, in particular, on the tunneling distance between the STM tip and the nanotube (typically a few Ångstrems). At the same time, according to the data in [2, 5] obtained from spectroscopy measurements on suspended nanotubes, the ratio $C_{tip}/C_{sub} \equiv C_L/C_R$ can be smaller as well as larger than unity depending on an effective length of the portion of the nanotube that is on the substrate (the effective length can be relatively short due to local defects induced by the edges of the trench). As a result, in the voltage-biased system, the position of the polaron level with respect to the chemical potentials of the leads is strongly affected by the ratio C_L/C_R. In the "reference frame" of the polaron level (where its position is voltage independent), the role of charging effects in the resonant tunneling problem can be viewed as follows: when changing the bias voltage $V = \mu_L - \mu_R$, the chemical potentials of the leads move in opposite directions with different "velocities" determined by c_R and $c_L = 1 - c_R$ for the left and right electrode, respectively.

In the case of highly asymmetric tunneling couplings, a simple physical picture can be developed to understand and predict (with some analytical results) phonon effects on the $I(V)$ characteristics. Generally, when the current is not zero, the bias-voltage window captures the polaron level accompanied by $N+M$ phonon sidebands, where the integer N (M) is defined as a number of phonon sidebands lying between the polaron level and the chemical potential of the electrode associated with the more (less) resistive junction:

$$N = \mathrm{Int}(|\mu_L - E|/\Omega) \ , \tag{2.8}$$

$$M = \mathrm{Int}(|\mu_R - E|/\Omega) \ , \tag{2.9}$$

where E is the position of the polaron level at zero bias. An example with $N = 2$ and $M = 1$ for $V > 0$ is shown on Fig. 2.2: due to high asymmetry $\Gamma_L \ll \Gamma_R$, only probabilities $\{P^0_m\}$ with $m \in [0, M]$ do not vanish in this limit. The probabilities

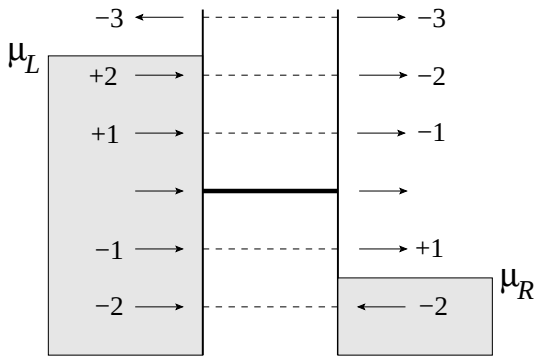

Figure 2.2: Energy-level diagram for the case $M = 1$ and $N = 2$; the arrows show possible channels for electrons to tunnel onto/from the dot with changing (indicated by numbers) the phonon occupancy; $\mu_L - \mu_R = V$

to have an electron on the dot with any n phonons, P^1_n, are suppressed due to "fast" tunneling of the electron to the right electrode via $n+2$ open channels; the probability to have the dot with an empty electron state but with the number of phonons $M + 1 = 2$ (and higher), P^0_{M+1}, is also negligible due to the "fast" tunneling of an electron from the right electrode with absorbing two phonons. In other words, on a large time scale determined by Γ_L^{-1}, the polaron-hole states with 0 and 1 phonon excitation are quasisteady states with respect to the tunneling coupling to the right electrode. The case $V < 0$ can be treated in the same manner where we obtain that only probabilities $\{P^1_m\}$ with $m \in [0, M]$ are not vanishing as Γ_L/Γ_R.

As a result, with a good accuracy, controlled by the smallness of Γ_L/Γ_R, the current flowing from the left to the right, $I \equiv I_L$, can be written as a sum of partial currents (I_m) representing M conducting channels which are distributed

with the corresponding phonon occupation probabilities:

$$I(V>0) = \sum_{m=0}^{M} P_m^0 \, I_m \ , \quad I_m = \Gamma_L \sum_{n=0}^{m+N} \gamma_{mn}^2 \ , \tag{2.10}$$

$$I(V<0) = -\sum_{m=0}^{M} P_m^1 \, I_m \ , \quad I_m = \Gamma_L \sum_{n=0}^{m+N} \gamma_{nm}^2 \ . \tag{2.11}$$

When varying V, the number of captured phonon sidebands, N and M, can change. In the voltage ranges where N and M do not change, we obtain plateaus in the $I(V)$ characteristics. When $V>0$ increases in such a way that only N changes (N can only increase with increasing V), the magnitude of each partial current, and hence the net current, will increase. Thus, we obtain here the positive differential conductance (PDC) behavior. On the contrary, if when increasing V only M changes (increases) while N remains constant, then a new phonon-assisted channel is added. This leads to redistribution of phonon occupation probabilities between all open channels: the net current may decrease, leading to a NDC behavior on $I(V)$.

As far as the bias voltage increases, the current eventually saturates and does not change in practice.

$I(V)$ characteristics: NDC versus PDC

Here we discuss the numerical solution of the rate equations exploring the parameter space in order to observe the signatures of NDC behavior. We mostly consider the case of the floating-level geometry ($E=0$) where the capacitances surrounding the dot fully specify the position of the polaron level.

Fig. 2.3 shows the $I(V)$ characteristics for different α's when c_L is small, so that the polaron level lies closer to μ_R. In the experiment of Refs. [1, 5], this means that the nanotube has a large overlap with the conducting substrate. As long as $M=0$, that is if $V<\Omega/c_L$ (this condition is satisfied on the bias-voltage range which is plotted), $P_n^0 \approx \delta_{n0}$, which results in the PDC behavior of $I(V)$. The PDC steps correspond to N increasing by 1 each time V passes through a multiple integer of Ω/c_R. Explicitly, the current-step amplitude at $V=n\Omega/c_R$ corresponding to the current increase is given by

$$\Delta I^{(n)} = \Gamma_L \, e^{-\alpha^2} \, \frac{\alpha^{2n}}{n!} \ . \tag{2.12}$$

For smaller α's the current-step amplitude decreases faster with increasing V, which leads to the saturation of the current at lower voltages. Note that the first step (low bias voltage) is rounded. This feature is specific to the fact that the capacitances are asymmetric: at small V, when the chemical potential of the lead with the largest capacitance remains close to the polaron level, thermally activated tunneling processes can be effective.

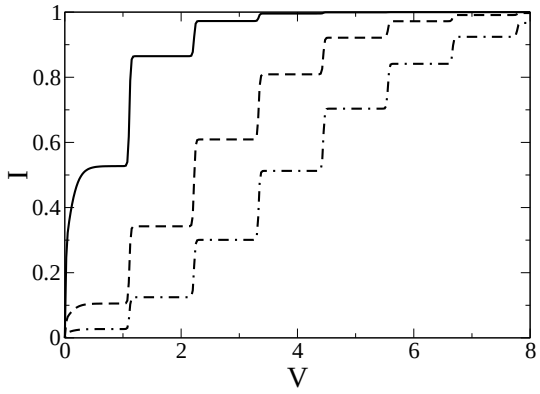

Figure 2.3: The case $c_L = 0.1$ for $\alpha = 0.8$ (solid), 1.5 (dashed) and 1.9 (dot-dashed). In all figures, the current I is plotted in units of $\Gamma_L\Gamma_R/(\Gamma_L+\Gamma_R)$, while the voltage V is given in units of Ω (we use $e = \hbar = 1$). We take $T = 0.01\,\Omega$, $E = 0$, and $\Gamma_L/\Gamma_R = 10^{-4}$ unless noted otherwise.

Fig. 2.4 shows the $I(V)$ characteristics for the "reversed capacitance" case corresponding to a relatively large c_L, when the polaron level is closer to μ_L. Within the plotted bias-voltage range, the current changes by steps when V passes through a multiple integer of Ω/c_L, as before. At these points, M increases by 1; correspondingly, one more phonon-assisted channel is added. For $\alpha = 1.5$ one still observes the PDC behavior, although the height of the current steps is strongly suppressed compared to the previous case on Fig. 2.3. For $\alpha < 1$ NDC occurs in the first step, and with decreasing α, more NDC steps appear.

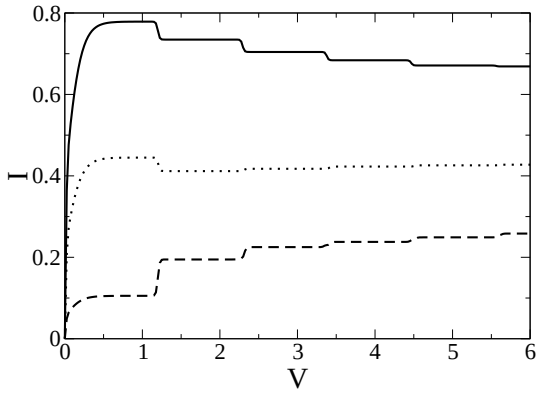

Figure 2.4: The case $c_L = 0.9$ for $\alpha = 0.5$ (solid), 0.9 (dotted) and 1.5 (dashed).

The phonon distributions P_m^0, which play the role of probabilities of open channels, at different bias voltages are shown on Fig. 2.5. This figure demonstrates the increase of the number of phonon excitations (far out of equilibrium) with increasing M in Eq. (2.9). It shows that at given V, the phonon occupation number is restricted by $M - 1$.

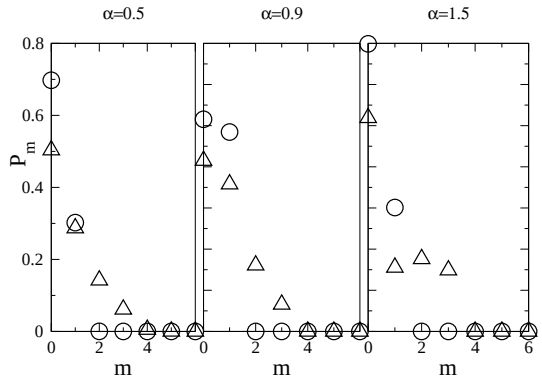

Figure 2.5: Phonon distribution, P_m^0, for the case of Fig. 2.4 at the bias voltage $V/\Omega = 2$ (circles) and 4 (triangles).

The possibility of NDC is not only restricted to the strongly asymmetric case $c_L \gg c_R$, but it can also be present in the more general situation when c_L and c_R are comparable, see Fig. 2.6. Notice that in this more general case, $I(V)$

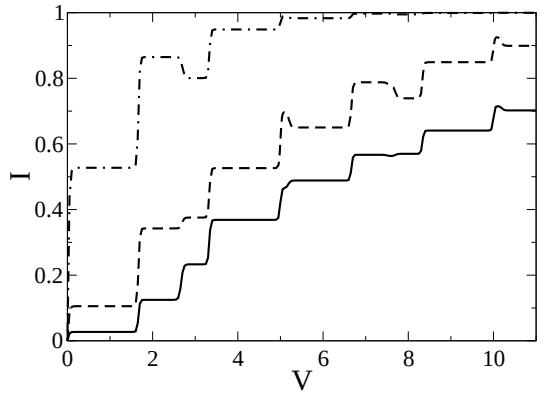

Figure 2.6: The case of $c_L = 0.4$ for $\alpha = 1.9$ (solid), 1.5 (dashed) and 0.8 (dot-dashed).

characteristics exhibit steps of different length. In the shown case of $c_R = 1.5c_L$, the number N of phonon sidebands above the polaron level increases by 1 with the voltage period $\Omega/c_R = (5/3)\,\Omega$; for these steps we *always* have a PDC behavior. At the same time, the number M of phonon sidebands below the polaron level increases by 1 with the voltage period $\Omega/c_L = 2.5\,\Omega$: one more channel becomes open which yields the possibility of NDC. The larger α, the more PDC-steps at low bias voltages are observed.

To demonstrate the role of asymmetry in the tunneling rates $\Gamma_{L,R}$ on current transport, in Fig. 2.7 we show $I(V)$ characteristics for the different cases of junction asymmetry. As is seen from the plots, the NDC steps in the cases of high and moderate asymmetry ($\Gamma_L/\Gamma_R = 0.01$ and 0.1, respectively) turn into PDC steps in the symmetric case ($\Gamma_L = \Gamma_R$). The height of the phonon-assisted steps in the asymmetric case is noticeably large compared to the symmetric one. This

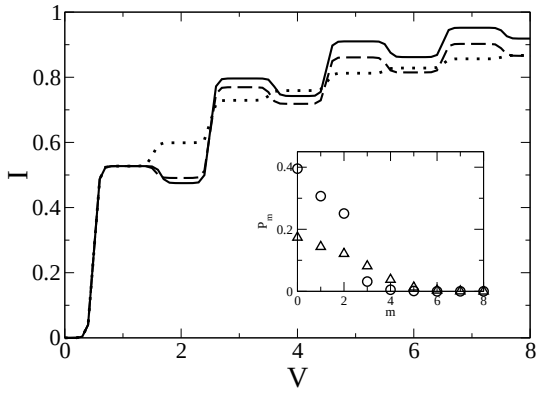

Figure 2.7: For $c_L = 0.5$, $\alpha = 0.8$, $T = 0.02\,\Omega$, and $E = 0.25\,\Omega$: $\Gamma_L/\Gamma_R = 10^{-2}$ (solid), 0.1 (dashed) and 1 (dotted). Inset shows the phonon distribution P_m^0 at the bias voltage $V = 4\,\Omega$ for $\Gamma_L/\Gamma_R = 10^{-2}$ (circles) and 1 (triangles).

is related to the phonon distribution, an example of which (at $V = 4\Omega$) is shown in the inset of Fig. 2.7. In the asymmetric junction, the number of phonons is restricted by M, while in the symmetric junction the phonon distribution is more spread out. As a result, in the symmetric case, the phonon-assisted contribution to the current is weakened.

Effect of the half–shuttle on $I(V)$ characteristics

We have also proposed that in a STM experiment, the tip-nanotube tunneling distance may deviate from its equilibrium value due to the "breathing" (radial) motion of the nanotube (see Fig. 2.1). Our model can easily be generalized to incorporate such an influence on the tip-nanotube coupling. Explicitly, we assume an exponential dependence of $\mathcal{T}_L$ on the boson coordinate $x = b + b^\dagger$:

$$\mathcal{T}_L(x) = \mathcal{T}_{L0}\, e^{-sx} \;, \tag{2.13}$$

where s is determined by the ratio of the amplitude of the zero-point RBM oscillations to the electronic tunneling length (≈ 0.5 Å) which characterizes the tunnel barrier between the STM tip and the nanotube. Such position-dependent amplitudes are usually introduced in the context of nanomechanical electronic devices [6], where one refers to the "shuttle" mechanism as the central region oscillates between the two electrodes. In our case, we refer to the "half-shuttle" effect, because only one of the tunneling amplitude (left) is modified by the position.

The half-shuttle can be detected by the asymmetry of the current-voltage curves: the presence of half-shuttle mechanism ($s \neq 0$) violates the parity symmetry of the current-voltage characteristics, leading to $I(V) \neq -I(-V)$.

Approaching the STM tip closer to the nanotube should strongly enhance the half-shuttle mechanism. According to our estimation, the amplitude of the zero-point RBM oscillations is of the order of 1 pm, which corresponds to $s \sim 0.1$. Fig.

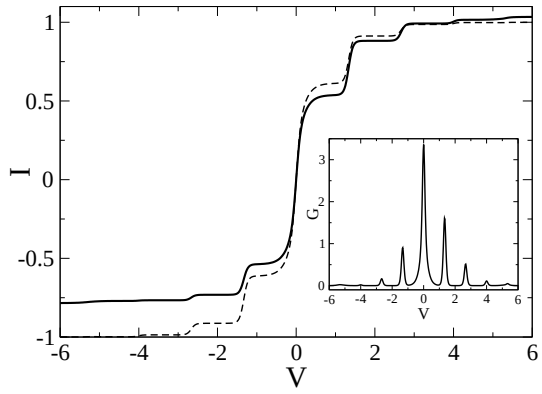

Figure 2.8: Asymmetry of $I(V)$ due to "half-shuttle": $s = 0.1$ (solid) and 0 (dashed). We take $\alpha = 0.7$, $c_L = 0.25$, $E = 0$, $T = 0.04\,\Omega$. The inset shows the differential conductance for $s = 0.1$.

2.8 shows $I(V)$ for the case when c_L is relatively small, which is favorable for PDC. The current steps are suppressed at negative voltages (differential conductance peaks in the inset of Fig. 2.8), while at positive bias voltage, the current steps have a tendency to increase. In other words, the half-shuttle mechanism works in favor of the formation of the polaron state: the probability of phonon-assisted tunneling onto the dot from the left electrode is increased, while the phonon-assisted tunneling from the dot to the left electrode is decreased.

The case of relatively large c_L is shown on Fig. 2.9. Like in the previous case, here we also observe suppression of the current steps at negative voltages. Numerically we have observed that when the poalron level is shifted, the "half-

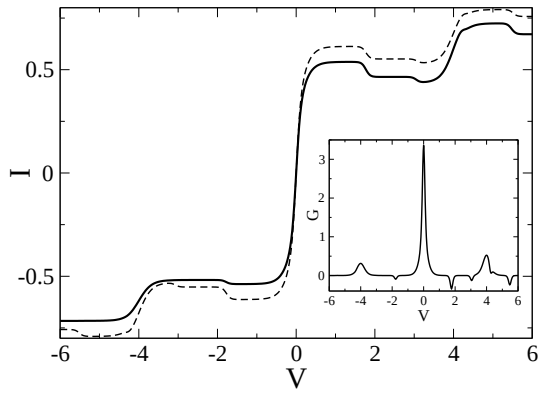

Figure 2.9: Same as Fig. 2.8 but for $c_L = 0.75$.

shuttle" mechanism tends to reinforce the NDC regions, but it cannot trigger this behavior on its own.

2.2 TRANSPORT IN THE POLARON CROSSOVER REGIME

There has been a large amount of theoretical work on the problem of tunneling through a resonant level coupled to a phonon mode. The approaches basically fall into two categories. The first category is the kinetic equation approach, which is relevant in the high temperature (or the weak tunneling) limit. Such an approach has been applied in Sec. 2.1. The second category deals with the opposite limit of low temperature (or the strong tunneling coupling). In this limit, the Landauer formulation of transport combined with the non-equilibrium Green function technique serves as a good starting point for computing transport. Depending on the strength of the electron-phonon coupling, various approximation schemes have been developed for weak electron-phonon coupling [7] and for the intermediate to strong coupling, where the electrons of the molecular quantum dot are dressed by a polaron cloud [8, 9, 10, 11, 12, 13, 14]. In paper VIII we go beyond the existing polaron approaches to molecular transport, allowing a better description of the intermediate electron-phonon coupling regime.

Perturbation theory is typically formulated in terms of (single) phonon Green functions. Yet when electron-phonon interaction is not weak, a more natural choice is to introduce a Green function which describes collective phonon excitations associated with the polaron cloud. We show that the electron spectral function of the molecular quantum dot can be evaluated systematically by diagram dressing of the polaron Green functions. With increasing tunneling coupling to the leads, correlations between polaron clouds become more important suggesting that phonon features for the current through the molecule could be more pronounced than expected. In particular, we have found that polaron-cloud correlations lead to a strong sharpening of the peak structure in the spectral function of the molecule: at relatively high temperature the phonon sideband peaks are much narrower than the tunneling coupling would suggest.

Keldysh Green function approach in the polaron representation

We use the same model as in Sec. 2.1 to describe a molecular quantum dot with a single-electron level coupled to a local vibration mode of frequency Ω. The Hamiltonian of the molecule coupled via tunneling to two metallic leads is given by $H = H_M + H_T + H_{leads}$ [see Eq. (2.1)], where the Hamiltonian of the molecule reads ($e = \hbar = 1$):

$$H_M = \left[\epsilon_0 - g \left(b + b^\dagger \right) \right] d^\dagger d + \Omega \, b^\dagger b \, . \tag{2.14}$$

We ignore the spin degree of freedom assuming a resonant tunneling situation in the Coulomb blockade regime, far from the Kondo regime. The bias voltage $V = \mu_L - \mu_R$ is imposed by shifting the chemical potentials (μ_j) of the leads, and we consider the symmetric junction with $\mathcal{T}_{L,R} = \mathcal{T}$.

In the steady state, the current through the junction can be expressed in terms of the nonequilibrium Green functions of the molecule, and is given by the Meir–Wingreen formula [15]:

$$I(V) = \Gamma \int \frac{d\omega}{8\pi} \, [f_L(\omega) - f_R(\omega)] \, iA(\omega) \, , \tag{2.15}$$

where $f_{L,R}(\omega)$ are Fermi distributions in the leads, Γ is the tunneling width of the dot level, and $A(\omega)$ is the Fourier transform of the electron spectral function of the molecule,

$$A(t-t') = -i\langle\{d(t),\, d^\dagger(t')\}\rangle \ , \tag{2.16}$$

which determines local electronic properties of the interacting region (molecule) in the presence of the leads.

As in Sec. 2.1, it is convenient to eliminate the electron-phonon coupling term in H_M by using the polaron transformation (2.5). As a result, the transformed tunnel Hamiltonian becomes dressed by the vibrations,

$$\tilde{H}_T = \sum_{jk} \mathcal{T}_k^* \, c_{jk}^\dagger D + h.c. \ , \tag{2.17}$$

where $D = dX$ and $X = e^{-i\alpha p}$ is the polaron cloud operator. This form of $\tilde{H}_T$ suggests an effective phonon-mediated coupling between the dot and lead electrons.

We now introduce the Keldysh Green function for the polaron, $\mathcal{G}(t-t') = -i \, \langle \, T_C\{ \, D(t)D^\dagger(t')\}\rangle$, where T_C is the Keldysh time-ordering over the Keldysh contour $\mathcal{C}$. Averaging over the leads yields:

$$\mathcal{G}(t-t') = -i \, \langle \, T_C\{S \, D(t)D^\dagger(t')\}\rangle_0 \, , \tag{2.18}$$

where $\langle \, ...\rangle_0$ denotes averaging over the states of the molecule only, and the effective S–matrix operator is given by

$$S = T_C \exp\left\{-i \int_{\mathcal{C}} d\tau d\tau' \, D^\dagger(\tau)\Sigma_0(\tau-\tau')D(\tau')\right\} \ . \tag{2.19}$$

The electron tunneling self-energy Σ_0 is built up from the Keldysh Green functions for the uncoupled leads, and can be expressed in terms of the tunneling coupling and electron distribution in the leads by virtue of $\Sigma_0^{<,>}(\omega) = \pm i \, (\Gamma/2) \sum_j \, f_j(\pm\omega)$.

The main challenge for the perturbation theory in Σ_0 resides in the fact that because the multi-phonon operator X accompanies the d operator in S, the Wick theorem is not applicable to express $\mathcal{G}$ in terms of the electron and phonon self-energies. It is nevertheless possible to develop a diagrammatic scheme and formulate the corresponding Feynman rules in the polaron representation. For this purpose, it is convenient to introduce a Keldysh Green function describing the polaron cloud:

$$\Lambda(t) = \langle \, T_C \left(X(t)X^\dagger(t')\right)\rangle_0 \ . \tag{2.20}$$

A typical approximation [16, 10, 12, 11], called the "single particle approximation" (SPA) in Ref. [13], consists in factorizing the electron Green function (2.18) as

$$\mathcal{G}(t-t') \simeq \mathbf{G}(t-t')\,\Lambda(t-t')\,, \tag{2.21}$$

where $\mathbf{G}$ obeys the Dyson equation for the dot in the absence of phonons. According to our analysis, this decoupling of electron and phonon dynamics can be justified in the anti-adiabatic regime [17], where Ω (and/or g) is large compared to Γ. The phonon mode is then fast and reacts instantaneously (on the time scale of Γ^{-1}) to the presence/absence of an electron on the molecule. The Feynman

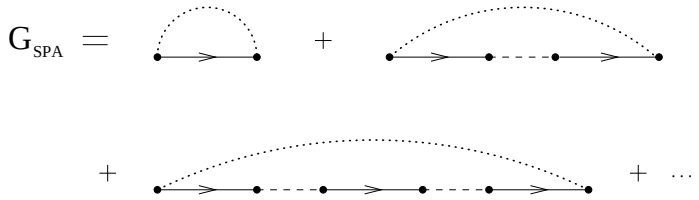

Figure 2.10: Dyson series for $\mathcal{G}$ corresponding to the SPA, Eq. (2.21): Electron propagator G (solid lines), self-energies Σ_0 (dashed lines), phonon-cloud dressing propagator Λ (dotted lines).

diagrams associated with the SPA are depicted in Fig. 2.10. In each order the phonon cloud connects only the end points of the full fermionic lines.

Although the series expansion of $\mathcal{G}$ in the tunneling self-energy Σ_0 (i.e., in Γ) is rather complicated in the presence of phonons, this expansion can be drastically simplified in the limit of $\mathrm{Re}\,\Lambda \gg \mathrm{Im}\,\Lambda$. Neglecting $\mathrm{Im}\,\Lambda$ turns out to be a good approximation even for the case of an intermediate electron-phonon coupling, $\alpha < 1$, and this result does not depend on temperature. Considering this case, we go beyond the anti-adiabatic regime and incorporate the effects of the polaron cloud in the vertex part of the Green function which are expected to become essential in the polaron crossover regime where Γ and Ω are comparable. Namely, in our treatment of the Dyson series for $\mathcal{G}$, we take into account correlations between phonon clouds corresponding to two sequential tunneling events of the lead electrons, which are happening on the time scale of the order of Γ^{-1}. In terms of the Feynman diagrams this is achieved by replicating the structure of the first order (in Γ) diagram: in all the higher orders, we keep only the nearest-neighbor crossing lines (representing Λ^{-1}) which connect the dressed electron propagators and the dressed self-energies. The diagrams associated with our expansion scheme, which is labeled as the "nearest-neighbor crossing approximation" (NNCA), are illustrated in Fig. 2.11. By summing up all the terms of perturbation theory within the NNCA, we derive a set of Dyson-type equations for the polaron Keldysh Green function, which is then used to calculate the spectral function of the molecule and/or the current.

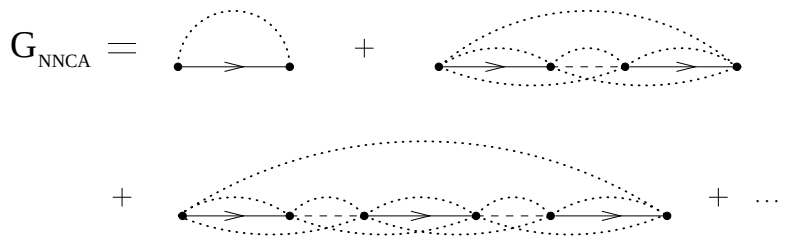

Figure 2.11: Diagrammatic representation of the NNCA. As in Fig. 2.10, dotted lines above the fermionic line represent the phonon-cloud dressing propagator Λ, while dotted lines crossing below the fermionic line represent the undressing corrections described by Λ^{-1}.

Calculation of the spectral function

Although, the dressed by phonons self-energy becomes voltage-dependent, inspection of this dependence shows that for $\alpha < 0.6$ the magnitude of the lead self-energy $\Sigma(\omega)$ is only slightly decreased compared to the bare one. Thus, for moderate α's the voltage dependence of the spectral function of the molecule can be discarded.

In Fig. 2.12 we plot the spectral function $A(\omega) = -2\mathrm{Im}\,\mathcal{G}^R(\omega)$ and the corresponding current calculated within the NNCA, and comparing with the SPA, for an intermediate coupling $\alpha = 0.4$. In order to reveal the polaronic effects, it is advantageous to assume that the leads have a lower temperature T_{leads} than that of the molecular quantum dot, T. In this situation, the leads act as a probe to detect the effect of vibrations on the electronic correlations on the molecule. When the molecule temperature is relatively high ($T > \Omega$), several satellite peaks appear in the spectral function (see Fig. 2.12) associated with emission/absorbtion of vibrational quanta. Although for small Γ, as expected, the NNCA and SPA results

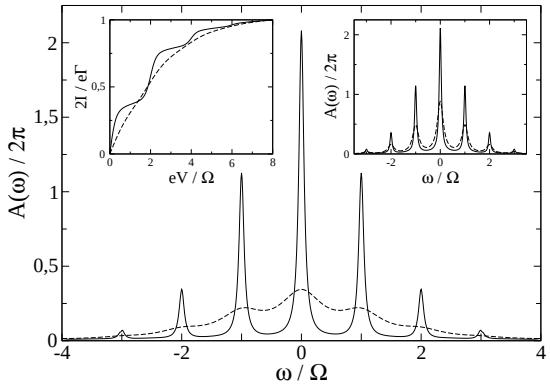

Figure 2.12: $A(\omega)$ at $T/\Omega = 4$ calculated within the NNCA (solid line) and SPA (dashed line), for $\alpha = 0.4$, $\Gamma/\Omega = 0.8$, and $\epsilon = 0$. Left inset: $I(V)$ characteristics for $T_{leads}/\Omega = 0.1$. Right inset: same as the main figure but for $2\Gamma/\Omega = 0.2$.

are hardly distinguishable (see right inset of Fig. 2.12), the difference is clearly

seen for the higher transparency (the main plot of Fig. 2.12). In this case, the current in the NNCA undergoes sharp steps corresponding to the phonon sidebands, while the current in the SPA does not show any structure (see left inset of Fig. 2.12). According to the NNCA, all excited satellite peaks remain sharp and are rather robust with respect to increasing Γ. This is the regime where the SPA breaks down. In this transition region, increasing the temperature acts in favor of the electron-phonon interaction which tends to localize the dot electron, leading to a well pronounced peak structure in the spectral function. This retardation effect is captured by taking into account correlations between phonon clouds in the NNCA. With increasing $\Gamma > \Omega$, we expect that the NNCA becomes less sufficient, and the higher order correlations between the polaron clouds should also be included.

The effect of suppression of the tunnel broadening in the spectral function at high temperature could be observed directly in the measurement of the differential conductance keeping the leads at very low temperature ($T_{leads} \ll \Omega$), so that $dI/dV \propto A(eV)$, but varying the local temperature of the molecule. For artificial molecules such as μm-sized carbon nanotubes, this could be achieved by local heating with a laser (with a spot size around 100 nm or less). The intermediate coupling regime has been realized in a recent experiment where the vibration corresponds to a stretching mode of the nanotube [3]. Laser heating may not be realistic for a true molecule because of the reduced size of the junction, but in the latter case it is reasonable to assume that molecule heating will still occur because of current flow (granted, these heating effects are not controlled, and are not described in the present model) implying some enhancement of phonon features in transport through the junction.

CHAPTER 3

SUPERCONDUCTING TRANSPORT THROUGH A VIBRATING MOLECULE

Molecular electronics is particularly exciting because of the possibility to contact molecules by leads of different nature. In this chapter, we discuss how electron transport is affected by a coherent phonon mode coupled to the molecular charge for the case of (s-wave) superconducting leads. Molecules connected to superconductors promise a rich terrain of exploration that allows for new spectroscopic tools (probing molecular properties), potentially useful applications, and interesting fundamental physics. First experimental results have already appeared for carbon nanotubes [18, 19, 20, 21] and metallofullerens [22].

3.1 INELASTIC MULTIPLE ANDREEV REFLECTION WITH PHONONS

So far transport through molecules has been theoretically studied only for normal leads, either using rate equations in the high-temperature regime, or perturbation theory in the electron-phonon coupling [7] in the quantum-coherent regime. While the combination of the vibrational coupling and correlation transport has barely been investigated in the context of supercurrent [23]. As it is well known for superconducting leads and large transmission through the junction, subgap transport is ruled by Multiple Andreev Reflection (MAR) processes [24]. These have been extensively studied for point contacts [25, 26, 27] and for junctions containing a resonant level [28, 29]. In paper IV, we provide a theoretical framework to include vibrations into superconducting transport through a resonant molecular level, and for the first time we establish a connection between the Keldysh formalism and the Landauer scattering approach for inelastic MAR. In the paper, we focus on the most interesting quantum-coherent low temperature limit with high transmission, where Coulomb charging effects are largely wiped out, and therefore can be neglected. We compute the dc current basically for the entire bias voltage range within a Keldysh Green function scheme valid for small electron-phonon coupling (g) but arbitrary phonon frequency (Ω).

Model and Keldysh approach

We choose a tractable model describing the relevant physics of a molecule sandwiched between two superconducting leads. The model Hamiltonian is given by (we put $e = \hbar = 1$ in intermediate steps)

$$H = \Omega b^\dagger b + \sum_\sigma (\epsilon_0 - gx) d_\sigma^\dagger d_\sigma + H_L + H_R + H_T \ , \tag{3.1}$$

where we consider one relevant (resonant) molecular level associated with the fermion operator d_σ for spin $\sigma = \uparrow, \downarrow$ and located at the energy ϵ_0. In Eq. (3.1) we take a linear coupling between the molecular charge and the phonon displacement $x = b + b^\dagger$. The leads ($j = L, R$) are described by a pair of standard s-wave BCS Hamiltonians, and the lead-molecule coupling is

$$H_T = \sum_{k,j=L/R=\pm} \psi_{jk}^\dagger \, \mathcal{T} \sigma_z e^{\pm i \sigma_z V t/2} \, d \ + \ \text{h.c.} \ , \tag{3.2}$$

where the bias voltage V enters via the time-dependent phase difference. Here we use Nambu spinor notations for electronic degrees of freedom,

$$\psi_{jk} = \begin{pmatrix} \psi_{jk,\uparrow} \\ \psi_{j,-k,\downarrow}^\dagger \end{pmatrix} \ , \quad d = \begin{pmatrix} d_\uparrow \\ d_\downarrow^\dagger \end{pmatrix} \ , \tag{3.3}$$

and σ_z is a standard Pauli matrix in Nambu space.

Because the calculation of MAR-dominated transport is already involved in the absence of phonons ($g = 0$), a nontrivial current-conserving self-consistent approach covering the large transmission limit seems out of question. The self-consistency is usually sufficient to ensure current conservation. However, we instead use a perturbation theory with the small expansion parameter g/Γ, where Γ is the tunneling half-width, assuming the electron-hole symmetric case, i.e., $\epsilon_0 = 0$, $\Gamma_{L,R} = \Gamma$, and $\Delta_{L,R} = \Delta$ (with Δ the superconducting gap), where current conservation is known to hold [30].

To compute the current-voltage characteristics, we employ the Keldysh Green function technique and calculate the Keldysh Green function for the d fermion,

$$\mathcal{G}_{\sigma\sigma'}(t, t') = -i \langle T_C [d_\sigma(t) d_{\sigma'}^\dagger(t')] \rangle, \tag{3.4}$$

where T_C is the time-ordering operator along the Keldysh contour. Similarly, we define a phonon Keldysh Green function $\mathcal{D}(t, t')$ for the phonon variable $x = b + b^\dagger$. Denoting the respective functions for $g = 0$ by $\mathcal{G}_0$ and $\mathcal{D}_0$, and using the self-energy diagrams in Fig. 3.1, the dressed Green functions used in our perturbative approximation follow from the Dyson equations:

$$\mathcal{G}^{-1} = \mathcal{G}_0^{-1} - \Sigma_{ph} \ , \tag{3.5}$$

$$\mathcal{D}^{-1} = \mathcal{D}_0^{-1} - \Pi \ . \tag{3.6}$$

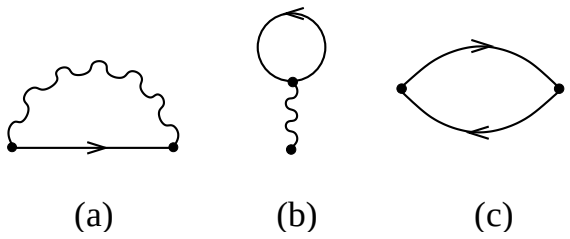

Figure 3.1: Self energy due to the presence of the phonon mode: (a) "Fock" and (b) "tadpole" diagram. The polarization bubble (c) leads to the dressed phonon propagator $\check{\mathcal{D}}$ (wiggly lines). Arrowed lines denote $\check{\mathcal{G}}_0$.

For numerical analysis, it is convenient to use the double Fourier representation

$$\mathcal{G}(t,t') = \sum_{n,m=-\infty}^{+\infty} \int_F \frac{d\omega}{2\pi}\, e^{-i\omega_n t + i\omega_m t'}\, \mathcal{G}_{nm}(\omega)\ , \tag{3.7}$$

and likewise for all other Green functions and self energies. Here $\omega_n = \omega + nV$ (n integer) for ω within the fundamental domain $F \equiv [-V/2, V/2]$. For fixed $\omega \in F$, the Dyson equations then take the form of matrix equations in the Fourier representation.

The dc current through the left/right junction is given by

$$I_{L/R} = \mp \mathrm{Re} \sum_{nm} \int_F \frac{d\omega}{2\pi}\, \mathrm{tr}\left[\sigma_z\, \Sigma_{L/R,nm}(\omega)\, \mathcal{G}_{mn}(\omega)\right]^{+-}\ , \tag{3.8}$$

where Σ_j is the electron self energy due to tunneling coupling to lead j, and the trace "tr" extends over Nambu space. Eq. (3.8) constitutes a generalization of the Meir-Wingreen formula [15] to the case of superconducting leads.

In paper IV, we establish a close connection between the above Keldysh Green function approach and a Landauer scattering approach incorporating *inelastic* transitions. Such an approach is formulated using the equation-of-motion method, where transfer matrices matching electron/hole scattering states in the presence of phonons are expressed in terms of Keldysh Green functions. The developed "inelastic MAR" picture is in fact essential in interpreting our numerical results.

Subgap regime: Inelastic MAR

Using Eq. (3.8), we have evaluated the I-V characteristics for $g = 0.15\Gamma$ and $k_B T/\Delta = 0.01$. Besides the current, we have also monitored the average phonon number $N_{ph} = \langle b^\dagger b \rangle$, which has always been less than 1, in accordance with our assumption of weak electron-phonon coupling.

We start with the subgap regime, where MAR provides the dominant transport mechanism. For $2\Delta/(n+1) < eV < 2\Delta/n$ (n integer), there is a total

number n of Andreev reflections for electrons (or holes) within the superconducting gap: an electron/hole is alternately retroreflected at the junction interfaces as a hole/electron, and each time a Cooper pair is passing through the junction.

The I-V curve for $\Gamma = 2\Delta$ and $\Omega = 0.2\Delta$ is given in Fig. 3.2, where the phonon contribution to the current $\delta I_{ph} \equiv I(g) - I(g = 0)$ is always negative. In this fully transmitting limit, the I-V curve for $g = 0$ is smooth and does not exhibit the MAR cusps encountered at lower transmission [25]. However, phonons *restore* such features near MAR onsets, with pronounced *even-odd parity effects*: For even (odd) n, δI_{ph} shows valleys (peaks) around $eV = 2\Delta/n$. This is clearly seen in the left inset of Fig. 3.2 for n up to 12. The appearance of even-odd parity oscillations is quite distinct and surprisingly regular given the complexity of this system.

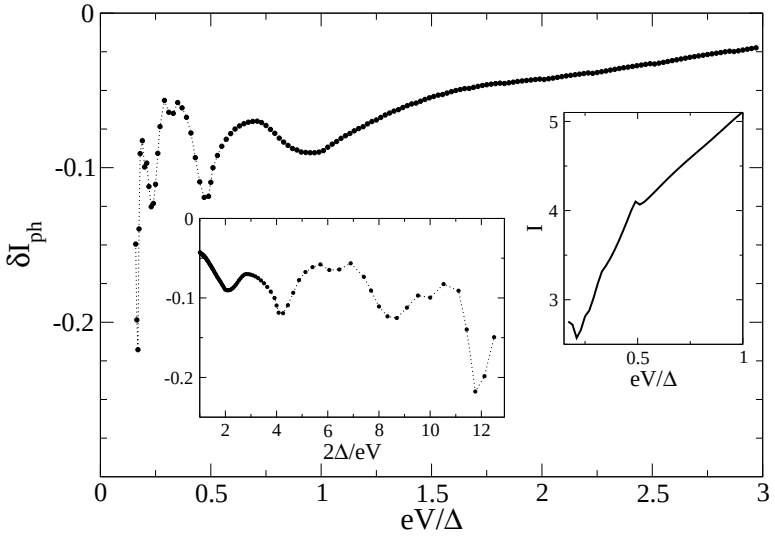

Figure 3.2: Phonon difference current $\delta I_{ph} \equiv I(g) - I(g = 0)$ for $\hbar\Omega = 0.2\Delta$ and $\Gamma = 2\Delta$. In all figures, currents are given in units of $e\Delta/(2\pi\hbar)$, and dotted lines are guides to the eye only. Left inset: Same as function of $2\Delta/eV$. Right inset: Part of the total I-V curve (note the scales).

In order to achieve a physical understanding of this even-odd effect, it is useful to invoke a MAR ladder picture in energy space, including inelastic transitions caused by phonon emission. A schematic description of the MAR ladder picture is given in Fig. 3.3: the two superconductors are positioned at the same chemical potential, but electrons (from left to right) and holes (from right to left) "climb" the MAR ladder by gaining eV for each Andreev reflection. The higher the total number of Andreev reflections in one cycle, the larger the total charge transmitted. Since we consider the high transmission limit where high-order MAR processes are not penalized, the current is therefore expected to increase (decrease) if phonon emission is able to increase (decrease) the number of Andreev reflections in a MAR cycle. For eV slightly below $2\Delta/n$ with *even* n, we then

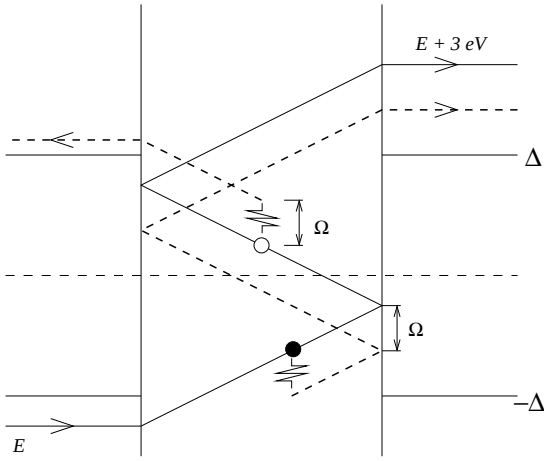

Figure 3.3: MAR ladder picture with phonon emission. Here eV is slightly below Δ: for an electron incoming from the left side, we have one hole (open circle) and two electron (filled circle) segments. Dashed lines indicate possible trajectories after single phonon emission involving either hole or electron segments. There is also a MAR path (not shown) for a hole entering from the right side, with one electron and two hole segments.

argue as follows (for $n = 2$, see Fig. 3.3). For small energy transfer $\hbar\Omega$, if a phonon is emitted during an electron segment, MAR trajectories in energy space are not drastically modified in the sense that the number of Andreev reflections stays unaffected. However, if a phonon transition occurs during a hole segment, the MAR ladder is shifted upwards by $\hbar\Omega$ and the last hole on the MAR ladder can be scattered into the continuum (left electrode in Fig. 3.3) instead of being Andreev reflected. Consequently, one Andreev reflection is lost and hence the current is expected to decrease. This argument applies both to incoming electrons and holes, and explains why current valleys are observed for $eV \approx 2\Delta/n$ with even n in Fig. 3.2. On the other hand, consider eV slightly above $2\Delta/n$ with *odd* n. Reiterating the above analysis, now phonon emission during a hole segment tends not to affect the number of Andreev reflections. If the phonon is emitted during an electron segment, however, an additional Andreev reflection has to take place to complete the MAR cycle, leading to a current peak for $eV \approx 2\Delta/n$ with odd n.

The I-V curve in the case of a high-frequency phonon mode, $\hbar\Omega = 1.8\Delta$, is shown in Fig. 3.4. Now δI_{ph} can be positive and again shows oscillations near the MAR onsets, which are less pronounced (cf. Fig. 3.2) for small $n = 2\Delta/eV$. Remarkably, even for small voltages, $eV \ll \hbar\Omega$, a rather complicated subgap structure is caused by the phonon. At such low voltages, this is only possible via MAR, for otherwise electrons or holes do not have enough energy to emit a phonon. The broad minimum corresponding to $n = 2$ observed in Fig. 3.2 has now vanished: for $eV < \Delta$, by emitting a high-energy phonon ($\hbar\Omega > \Delta$), the last

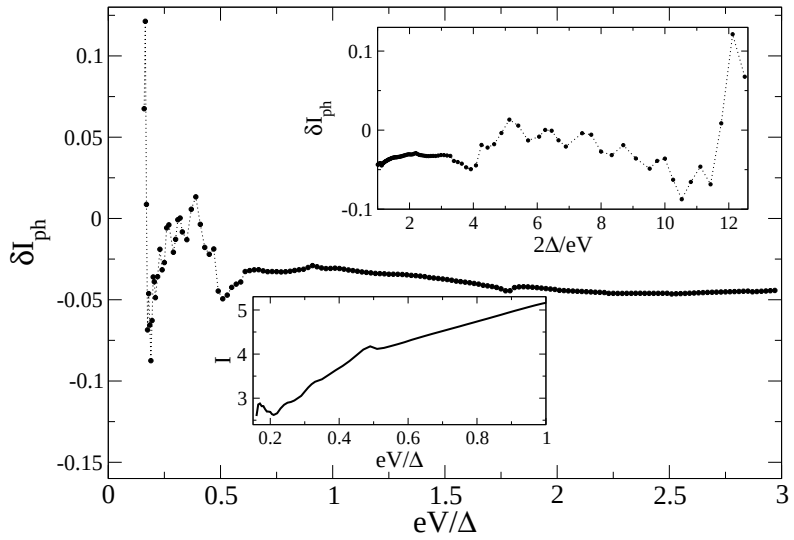

Figure 3.4: Same as Fig. 3.2 but for $\hbar\Omega = 1.8\Delta$. The upper inset gives δI_{ph} as a function of $2\Delta/eV$, the lower inset gives the low-voltage part of the total current.

electron on the MAR ladder can now be scattered back inside the gap instead of heading to the continuum. This increases the number of reflections and thus the current. As a phonon emitted during the hole segment has the opposite effect, the net outcome of the higher phonon frequency is to suppress the valley at $eV \approx \Delta$ expected for small Ω. Figure 3.4 also shows a dip in the current at $eV \approx 1.8\Delta$, representing a phonon backscattering feature at $eV = \hbar\Omega$.

Excess and Josephson current

We have also computed the difference $\delta I_{exc,ph}$ between the excess currents I_{exc} with and without the phonon. For the case of high transmission encountered here, we have found that phonons generally *enhance* the excess current. To give a concrete example, for $\hbar\Omega = 0.8\Delta$, $\Gamma = 2\Delta$ and $g = 0.5\Delta$, we find $\delta I_{exc,ph}/I_{exc} \approx 0.07$. A similar current enhancement at high transmission was also found for environmental Coulomb blockade in superconducting junctions, and has been explained as "antiblockade" effect [31]. As such, this effect of the phonon mode may not be too surprising.

By adopting our approach to the Matsubara representation, we have also calculated the equilibrium Josephson current flowing through the vibrating molecule. For arbitrary parameters, it is straightforward to numerically compute the full current-phase relation $I(\phi)$. However, in the *adiabatic* phonon regime defined by

$$\hbar\Omega \ll \Delta \ll \Gamma \ , \tag{3.9}$$

the current-phase relation can even be calculated analytically. We have found

that the Josephson current is given by

$$I(\phi) = (e\Delta^2/2\hbar)\ D\sin(\phi)/E_a(\phi)\ , \tag{3.10}$$

where

$$E_a(\phi) = \Delta[1 - D\ \sin^2(\phi/2)]^{1/2} \tag{3.11}$$

is an Andreev bound state energy in the junction with an effective transparency

$$D = \frac{1}{1 + (g/2\Gamma)^2}. \tag{3.12}$$

The ϕ-dependent shift without any broadening of the Andreev level caused by the coupling to a phonon mode is characteristic for the coherent limit and decreases the critical current. Very similar results were reported in Ref. [23], where the opposite limit $\Gamma \ll \Delta$ has been studied by lowest-order perturbation theory in the molecule-lead hopping.

3.2 PHONON SQUEEZING BY JOSEPHSON CURRENT

Nanoelectromechanical (NEM) systems have been a subject of extensive research in recent years. The possibility of combining electrical and mechanical degrees of freedom on the nanoscale may give rise to technological advances as well as manifestations of fundamental physical phenomena. In particular, a challenging goal consists in creating *non-classical vibrational states*, similar to non-classical states of light, with reduced quantum fluctuations in one of the mode quadratures, the so-called squeezed states. Besides the fundamental interest, this would also allow to exploit the quantum properties of mechanical degrees of freedom for applications in areas such as weak force detection, precision measurement, and quantum information processing. The generation of squeezed states in bulk materials was proposed in [32, 17, 33]. Recently, different squeezing scenarios have been suggested for nanomechanical resonators driven by nonlinear couplings [34, 35, 36, 37].

The excitation of molecular vibrations by an electronic current has been observed with normal metallic leads in several molecules including fullerenes and carbon nanotubes [38, 39]. The latter are in fact NEM systems, where charge fluctuations are coupled to bending [40], stretching [3] or radial breathing modes (RBM) [1]. Incoherent polaronlike charge fluctuations due to transport trigger a nonequilibrium distribution of the phonon mode. In paper V, we address the superconducting regime, and show that, for transparent lead-molecule contacts, the Josephson effect survives a strong electron-phonon interaction and triggers coherent phonon fluctuations. As a striking consequence, the conjugate momentum of the molecular distortion displays reduced zero-point fluctuations (squeezing), including nearly Gaussian minimum-uncertainty states. The magnitude of the phonon squeezing can be controlled by varying the superconducting phase difference, and is also sensitive to the junction asymmetry.

Squeezed states

The concepts of coherent and squeezed states were both elaborated mainly in the context of quantum optics. A coherent state is a phase-coherent sum of (photon) number states. In this state, the quantum fluctuations in any pair of conjugate variables are at the lower limit of the Heisenberg uncertainty principle. In other words, a coherent state is as "quiet" as the vacuum state. Squeezed states are interesting because they can have smaller quantum noise than the vacuum state in one of the conjugate variables (quadratures).

For a harmonic oscillator described by the Hamiltonian $H_{osc} = \Omega b^\dagger b$, a general class of Gaussian minimum-uncertainty squeezed states is defined as follows [41]:

$$|\lambda, \eta\rangle = D(\lambda)S(\eta)|0\rangle \ , \tag{3.13}$$

where $D(\lambda) = \exp\left(\lambda b^\dagger - \lambda^* b\right)$ is a displacement operator, and

$$S(\eta) = \exp\left[(\eta^*/2)b^2 - (\eta/2)b^{\dagger 2}\right] \tag{3.14}$$

denotes the squeezing operator. The state $|\lambda = 0, \eta\rangle$ is referred as the squeezed vacuum state, and the absolute value of $\eta = \rho\, e^{i\theta/2}$ is called the squeezing parameter. For vacuum squeezed states, the quadrature components $x_{1,2}$, defined by $b = e^{i\theta/2}\left(x_1 + ix_2\right)/2$, fulfill the uncertainty relation $\delta x_1\, \delta x_2 \geq 1$, where the variance of one component, $\delta x_1 = e^{-r}$ is reduced below the standard quantum limit of 1, whereas the noise in the other component is enhanced, $\delta x_1 = e^r$. Because of these properties, squeezed states form an exciting group of states that can provide unique insight into quantum mechanical fluctuations.

A familiar method in quantum optics to generate a squeezed state of a harmonic oscillator is to use a parametrically driven nonlinear potential corresponding to the Hamiltonian

$$H_{osc,p}(t) = \Omega\, b^\dagger b + \zeta(t)b^{\dagger 2} + \zeta^*(t)b^2 \, . \tag{3.15}$$

For NEM systems, the application of this method has been proposed in [34], but the requirements, a sufficiently strong nonlinearity to overcome the losses, and preparation of an initial state close to the ground state of harmonic oscillator, are not easily to met.

Another method of introducing nonlinear terms to produce squeezing is to couple a harmonic oscillator to a two-level system. Such a scenario but in the context of "engineering" dissipation has been suggested in [35] by coupling a nanoresonator to a Cooper pair box (the latter plays the role of a dissipative two-level system). In paper V, we suggest an alternative scenario to generate squeezing by employing a true microscopic two-level system: coherent nonlinear effects in a molecular conductor are realized due to the interaction between the phonon mode and a pair of Andreev (subgap) states formed in the junction region by the gradient of the superconducting phase.

Effective spin–boson Hamiltonian

We consider a simple resonant-level model describing the electron level ϵ_0 coupled to two superconducting electrodes. The electron on the resonant level is linearly coupled to a single vibrational mode (phonon) with frequency Ω. The model Hamiltonian is $H = H_M + H_L + H_R + H_T$, where H_M, $H_{L,R}$ and H_T, respectively, describe the uncoupled molecule, the superconducting leads and the molecule-lead coupling. Explicitly, the Hamiltonian of the molecule reads (we use $\hbar = e = 1$):

$$H_M = \left[\epsilon_0 - g\left(b + b^\dagger\right)\right](n_\uparrow + n_\downarrow) + U n_\uparrow n_\downarrow + \Omega\, b^\dagger b\,, \tag{3.16}$$

where $n_\sigma = d_\sigma^\dagger d_\sigma$ is the occupation number operator for spin $\sigma = \uparrow, \downarrow$, and U is the repulsive Coulomb interaction for electrons on the molecule. As in Sec. 3.1.1, the leads are described by standard BCS Hamiltonians, and the molecule-lead coupling is given by

$$H_T = \sum_k \sum_{j=L/R=\pm} \psi_{jk}^\dagger\, \mathcal{T}_j\, \sigma_z e^{\pm i\sigma_z\phi/4}\, d \;+\; \text{h.c.}\,, \tag{3.17}$$

with ϕ the superconducting phase difference across the junction.

We assume that the position of the molecular dot level is tuned by a gate voltage close to the degeneracy point so that, in the limit $U \to \infty$, the single occupied dot states ($n_\uparrow + n_\downarrow = 1$) are taken out, and do not contribute to the charge dynamics. Then, assuming that the superconducting gap Δ is the largest energy left in the problem, $\Delta \gg \Omega$, g, Γ_j (Γ_j is the dot-level half-width due to tunneling coupling to lead j), we focus on the molecule dynamics restricted to the subgap energy domain, and neglect quasiparticle excitations in the leads (at low temperature).

Using an imaginary time path-integral representation of the partition function, we derive an effective Hamiltonian describing the low-energy physics of the molecular junction by tracing out the electronic degrees of freedom of the leads. After introducing the Pauli-matrix operators $\tau_z = |0_d\rangle\langle 0_d| - |\uparrow\downarrow\rangle\langle\uparrow\downarrow|$ and $\tau_+ = (\tau_-)^\dagger = |0_d\rangle\langle\uparrow\downarrow|$ for the 0 and $2e$ charge states ($|0_d\rangle$ and $|\uparrow\downarrow\rangle$, respectively), we arrive at the effective spin-boson Hamiltonian (in the charge representation):

$$H_{eff} = \Omega\, b^\dagger b - \left[\epsilon - g\left(b + b^\dagger\right)\right]\tau_z + E_a(\phi)\,\tau_x\,, \tag{3.18}$$

with

$$E_a(\phi) = \Gamma\left[\cos^2(\phi/2) + \gamma^2 \sin^2(\phi/2)\right]^{1/2}\,, \tag{3.19}$$

where $\Gamma = \Gamma_L + \Gamma_R$, $\gamma = (\Gamma_L - \Gamma_R)/\Gamma$ quantifies the junction asymmetry, and ϵ is determined by detuning from the charge degeneracy point. Eq. (3.19) yields the (phase-dependent) spectrum of Andreev levels, $\pm E_a(\phi)$, with a gap when $\gamma \neq 0$.

Any eigenstate of H_{eff}, in particular, the ground state $|\Psi_0\rangle$, exhibits entangled charge and vibrational states:

$$|\Psi_0\rangle = \sum_{n=0}^{\infty}\left(A_n^{(0)}|0_d\rangle + A_n^{(2)}|\uparrow\downarrow\rangle\right)|n\rangle\,, \tag{3.20}$$

where $|n\rangle$ is the n-phonon Fock state. It is worth to be mentioned that at the degeneracy point ($\epsilon = 0$) the 0 and $2e$ charge amplitudes in (3.20) are not independent but related by $A_n^{(0)} = (-1)^{n+1} A_n^{(2)}$, owing to the parity symmetry $\left[H_{eff}\,,\, \tau_x(-1)^{b^\dagger b}\right] = 0$.

In the ground state, the relevant experimental quantity is the current expectation value, $J(\phi) = \langle\Psi_0|\hat{J}(\phi)|\Psi_0\rangle$, which probes the overlap of phonon states. Using a method of generating functional, we have derived an expression for the effective current operator $\hat{J}(\phi)$, which in spin notation takes the form:

$$\hat{J}(\phi) = \frac{\Gamma}{2\rho(\phi)} \left[\left(1-\gamma^2\right) \sin\phi \;\tau_x + 2\gamma\,\tau_y \right], \tag{3.21}$$

with $\rho(\phi) = E_a(\phi)/\Gamma$. Note that in the presence of phonons, the current operator does not commute with the Hamiltonian (3.18). This results in phonon-induced fluctuations of the current even in the symmetric case $\epsilon = \gamma = 0$.

Nonclassical phonon states

One type of nonclassical phonon states can be produced in the limit of weak tunneling coupling $\Gamma \ll \Omega,\, g$, where it is convenient to perform a unitary transformation $U_\alpha = e^{-i\alpha p \tau_z}$, with $\alpha = g/\Omega$ and $p = i(b^\dagger - b)$, on H_{eff}, resulting in

$$\tilde{H}_{eff} = \Omega b^\dagger b \,-\, \epsilon\tau_z + E_a(\phi)\,\left[\cos(\alpha p)\,\tau_x + \sin(\alpha p)\,\tau_y\right]\,. \tag{3.22}$$

To lowest order in Γ/Ω, for $\epsilon = 0$, one obtains the ground state

$$|\Psi_0\rangle = e^{i\chi/2}|\alpha\rangle|\,0_d\rangle - e^{-i\chi/2}|-\alpha\rangle|\uparrow\downarrow\rangle\;, \tag{3.23}$$

where $|\pm\alpha\rangle = D(\pm\alpha)|0_{ph}\rangle$ are opposite coherent states of the phonon mode. Now, by projecting $|\Psi_0\rangle$ onto one of the current eigenstates, $|\pm\rangle$, the molecule can be put into a superposition of "spatially" separated vibrational states:

$$|\Phi_\pm\rangle = \left(e^{i\chi/2}|\alpha\rangle \pm e^{-i\chi/2}|-\alpha\rangle\right)/\sqrt{2}\;. \tag{3.24}$$

These states are similar to the "cat states" generated in quantum optics. The relative phase factor entering the superposition is determined by the junction asymmetry, $\chi = \arctan\left(\gamma\tan(\phi/2)\right)$. Interestingly, for $\gamma = 0$, the states $|\Phi_\pm\rangle$, linked to the oppositely flowing current states ($|\pm\rangle$, respectively), are built from phonon Fock states with even/odd occupation numbers only.

For small Γ, the resulting coherent states, $|\pm\alpha\rangle$, are not squeezed, i.e., squeezing marks a deviation from the displaced oscillator states. However, the possibility of the generation of Gaussian squeezing can already be seen from the Hamiltonian (3.22) by expanding it in small α: this yields the term proportional to $b^2 + b^{\dagger 2}$ which is precisely the one exploited in the Hamiltonian (3.15) to generate two-phonon squeezed states.

In order to probe the generic squeezing properties of the molecular phonon, we compute the mean square fluctuations, δx and δp, of both the displacement coordinate $x = b + b^\dagger$ and the conjugate momentum p assuming zero temperature. Fig. 3.5 shows the ϕ-dependent variation of the momentum fluctuation δp as well as the uncertainty $\delta x \delta p$. (The ground-state value of $\delta x \delta p$ for an harmonic oscillator is 1.) Coherent charge fluctuations enhance the fluctuations of x beyond

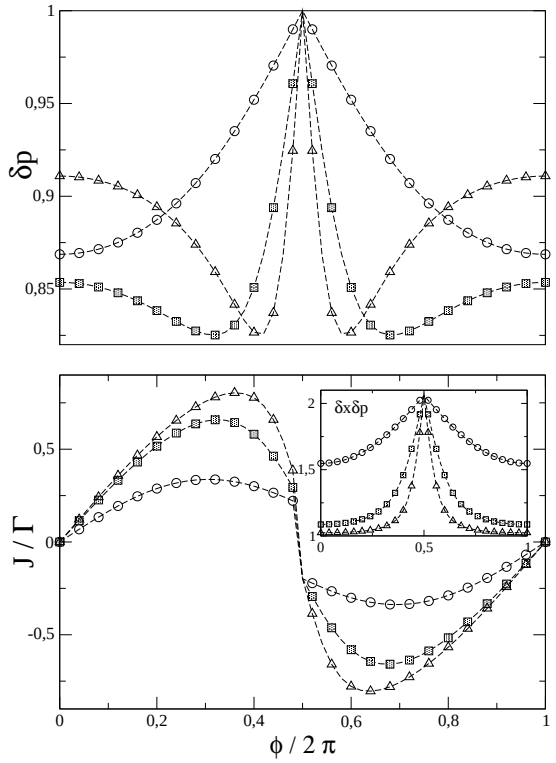

Figure 3.5: (a) Squeezing of the momentum and (b) Josephson current as functions of the phase difference ϕ. We take $\Gamma/\Omega = 0.5$ (circles), 2 (squares), and 4 (triangles) for $g/\Omega = 0.9$, $\epsilon = \gamma = 0$. The inset in (b) shows the Heisenberg uncertainty as a function of ϕ.

the quantum zero-point magnitude, whereas the fluctuations of the momentum p are *reduced*. Squeezing ($\delta p < 1$) occurs for a wide range of parameters, and its intensity depends on ϕ, in accordance with the effective polaronic interaction constant $g^2/E_a(\phi)$ of the spin-boson Hamiltonian (3.18). In general, squeezing does not involve minimum-uncertainty states. Yet, $\delta x \delta p = 1$ can be made very close to unity for intermediate g and Γ (see the inset of Fig. 3.5 b).

Squeezed states can only be produced with a sizeable Josephson current. To illustrate this, in Fig. 3.6(a) the Josephson current is plotted as a function of the bare electron-phonon interaction: as expected, J decreases but moderately if g is not too large. The inflexion region corresponds to the polaron crossover where optimum squeezing (in the sense of minimum-uncertainty) is achieved.

Interestingly, the asymmetry $\gamma \neq 0$ leads to strong (up to 40%) and nearly harmonic squeezing, having a weak dependence with the phase difference, see Fig. 3.6(b).

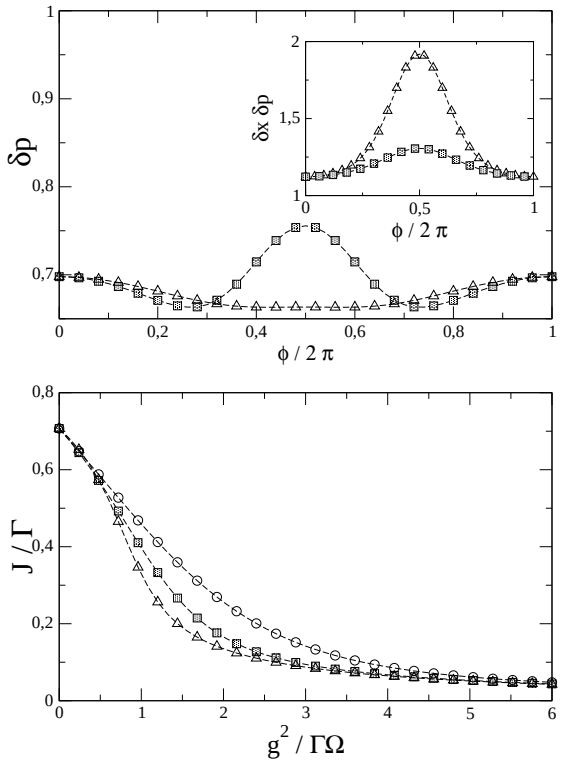

Figure 3.6: (a) Josephson current as a function of the electron-phonon interaction, at $\phi = \pi/2$: $\Gamma/\Omega = 0.5$ (circles), 1 (squares) and 2 (triangles) for $\epsilon = \gamma = 0$; (b) Same as Fig. 1a, but in the asymmetric case: $\gamma = 0.5$ (squares) and 0.75 (triangles) for $g = 1.5$, $\Gamma = 4\Omega$, $\epsilon = 0$.

To check that the squeezing property is not only restricted to the limit of large Δ, we have analyzed the case of finite Δ by using a variational ansatz approach [32]. For finite Δ, squeezing is still present provided that $g > \Omega$. For instance, with the parameters of Fig. 3.6(b) ($g = 1.5\Omega, \Gamma = 4\Omega, \gamma = 0.75$), at $\phi = 0$ we have obtained $\delta p = 0.76$ for $\Delta = 4\Omega$. In the limit of $\Delta \ll \Gamma$, assuming $\Delta = 0.1\Omega$, $g = 1.2\Omega$, $\Gamma = 2\Omega$, and $\gamma = 0$, we have obtained (at $\phi = \pi/2$) $\delta p = 0.77$ with $\delta x \delta p = 1.1$, indicating that even with rather high frequency modes such as RBM in nanotubes ($\Omega \approx 10meV$), squeezing can be produced (assuming Nb contacts, $\Delta \approx 1meV$).

The squeezing is expected to be robust against environmental effects induced by coupling the local phonon mode to external vibrations (playing the role of a phonon bath). Provided that the quality factor Q is large enough ($Q \sim 10^2 - 10^4$ has been suggested [40, 3, 1]), the squeezing property of the ground state is protected by the relatively large gap ($\sim \min(\Omega, \Delta)$) in the excitation spectrum

of the system.

Detection of squeezed phonon states

We have proposed a simple scheme to detect squeezed phonon states. Optical detection techniques may be used, such as Resonant Raman Scattering (RRS), which has been achieved in carbon nanotubes [42] for RBM modes. In RRS, the incident photon (with frequency ω) excites an electronic transition within the molecule, and a photon is reemitted with excitation of the phonon mode (see Fig. 3.7). We denote d' the state corresponding to a low-lying molecular orbital, which is assumed to be decoupled from the molecular vibrations. The molecule Hamiltonian then reads:

$$H'_M = H_M + \epsilon' d'^{\dagger} d' + \left(\zeta_\omega e^{-i\omega t}\, d^\dagger d' + H.c.\right) . \tag{3.25}$$

In calculating the Raman transition rate, we assume that the initial state is the projection of the ground state (3.20), $|\Psi_0\rangle \equiv |\Phi^{(0)}\rangle|0_d\rangle + |\Phi^{(2)}\rangle|\uparrow\downarrow\rangle$, on the zero-electron subspace, $|i\rangle = |\Phi^{(0)}\rangle|0_d\rangle|\uparrow\downarrow\rangle_{d'}$, with the phonon part $|\Phi^{(0)}\rangle = \sum_{n=0}^{\infty} A_n^{(0)}|n\rangle$, while the final state with *one* electron in the orbital d (together with a hole in the orbital d') is given by $|f\rangle = |n\rangle|\sigma\rangle_d|-\sigma\rangle_{d'}$. Thus, resonant

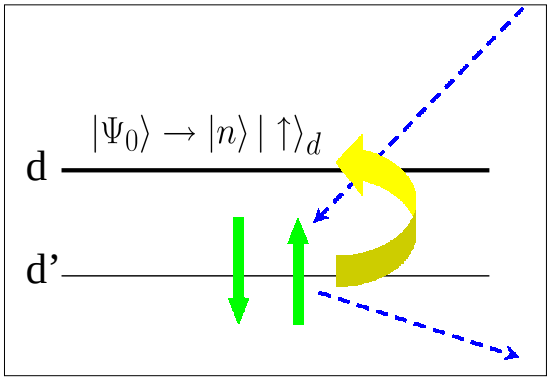

Figure 3.7: Schematic picture of resonant Raman scattering process which induces an electronic transition (shown for spin "up" in the picture) from low-lying molecular orbital d'. As a result of this transition, the state $|\Psi_0\rangle$ of d orbital collapses into a single-electron state with n phonons. Dashed-line arrows indicate an incident and reemitted photons.

Raman emission lines (Stokes) will appear at energies $\epsilon_0 - \epsilon' + n\Omega - E_0$ (E_0 is the ground state energy corresponding to $|\Psi_0\rangle$), with probabilities given by $\langle n|\Phi^{(0)}\rangle^2 = |A_n^{(0)}|^2$; this yields a spectroscopy of the squeezed state $|\Phi^{(0)}\rangle$. While absorption from a filled molecular orbital (d') probes $|\Phi^{(0)}\rangle$, similarly absorption towards an empty (high-lying) orbital will probe $|\Phi^{(2)}\rangle = \sum_{n=0}^{\infty} A_n^{(2)}|n\rangle$ by taking out an electron from the state $|\uparrow\downarrow\rangle_d$.

CHAPTER 4

JOSEPHSON CURRENT THROUGH A MAGNETIC QUANTUM DOT

4.1 JOSEPHSON π JUNCTION WITH MOLECULAR SPIN

Of great importance for molecular spintronics are the molecules possessing a large spin, or "single molecule magnets". Such molecules can now be synthesized, for example, the molecule $Mn_{12}Ac$, which has a ground state with a large spin $S = 10$, and a very slow relaxation of magnetization at low temperature [43]. In paper VI, we study the equilibrium properties of a molecule with a large magnetic moment placed between two superconductors under condition of the Josephson effect, when a Josephson current flows through the molecule. The focus is on the influence of the spin coupling on the Josephson effect. We show that when the spin coupling is large enough, the superconducting junction behaves as a π junction, with a reversal of the Josephson current compared to the case with no spin coupling. The mechanism leading to the π-shift can be explained in terms of contributions of the Andreev bound states and of the continuum of states above the superconducting gap. The continuum contribution to the current is essential to understand the π junction behavior. The π-shift can be reversed by varying the system parameters, e.g., the position of the quantum dot level, implying a controllable π junction with novel application as a Josephson current switch.

Brief history of the π-shift

In order to show how our work and results differ from the existing works on π junctions, it is useful to outline the history of π-shift. π junctions were first proposed theoretically by Bulaevskii and coworkers in [44]. They considered a tunnel junction with magnetic impurities in the barrier. In this system π junction behavior is produced by spin-flip tunneling processes. As a result, a super-conducting ring containing a π junction may generate a spontaneous current and a magnetic flux opening the way for experimental detection. Actually, it was Kulik who in 1966 was the first to discuss the spin-flip tunneling through an insulator with magnetic impurities [45]. The spin-flip tunneling is predicted to dominate the conventional

Josephson current when the spin coupling in the barrier is strong enough. In a superconductor–quantum dot–superconductor junction (S-QD-S), changes in the sign of the critical current can be observed as a function of the quantum dot gate voltage which controls the occupancy of the dot. Due to this gating capability one has more control over the magnetic state of the junction compared to a magnetically doped Superconductor-Insulator-Superconductor junction [46]. Superconductor-ferromagnet-superconductor (SFS) junctions have also been shown to give rise to a π junction behavior both in theory [47] as well as in experiments [48]. The study of the superconducting π state sheds more light on the coexistence of superconductivity and ferromagnetism in general and is also important for superconducting electronics [49]. In contrast to SFS systems, π junction behavior in superconductor–normal metal–superconductor (SNS) systems occurs due to the creation of a non-equilibrium distribution of electrons in the barrier via a control channel [50]. Finally, π junctions have been theoretically predicted and experimentally observed in superconducting d-wave junctions [51].

Generally, in works related to π junction behavior, the contribution to the Josephson current from the quasiparticle continuum states is ignored, which can be justified in the case of short (compared to the superconducting coherence length) SNS junctions [52] and quantum point contacts. The necessity of taking into account the continuum current for relatively long junctions has recently been stressed in [53, 54, 55]. In paper VI, we calculate explicitly the contribution from the continuum in a S-QD-S junction and show that the in the presence of a strong coupling to the molecular spin the continuum current plays an essential role in understanding the π junction behavior.

Model Hamiltonian

The model system under consideration is illustrated in Fig. 4.1. We model the molecule as a quantum dot with a single electron level (ϵ) coupled to two superconducting leads. The single level is coupled to the molecular spin $\mathbf{S}$ through the on-site exchange interaction $J\mathbf{S}\cdot\mathbf{s}$, where $\mathbf{s}$ is the electronic spin on the molecule, and J is the exchange coupling constant. We neglect the interaction of the spin with the leads. In view of long relaxation times of large magnetic spins, we treat the molecular spin as a fixed quantity, which plays the role of a local magnetic field for the electrons passing through the molecule. The model Hamiltonian then reads:

$$H = \epsilon \sum_{\sigma} d_{\sigma}^{\dagger} d_{\sigma} + JS\left(d_{\uparrow}^{\dagger} d_{\uparrow} - d_{\downarrow}^{\dagger} d_{\downarrow}\right) + H_L + H_R + H_T \ , \tag{4.1}$$

where we chose the z axis along the molecular spin orientation. We use the same notation as in the previous chapter. In Eq. (4.1), $H_{L,R}$ and H_T, respectively, describe the (s-wave BCS) superconducting leads and the molecule-lead coupling. The latter is given by Eq. (3.17).

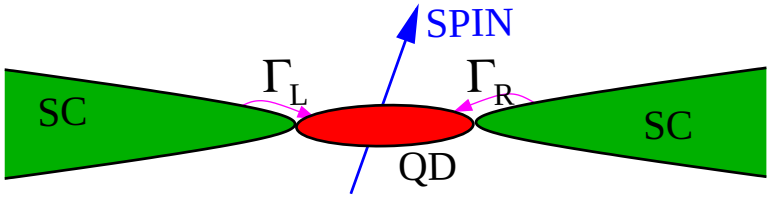

Figure 4.1: Schematic view of a Josephson quantum-dot (molecule) device with magnetic spin.

In our model, we neglect the charging energy of the molecule. This can be justified when the dot level is tuned to the charge degeneracy point (cf. Sec. 3.2.2), or when the on-site repulsion is small compared to the tunneling width Γ: the dwelling time of electrons on the molecule is so short that charging effects do not have time to operate.

Andreev bound states and continuum current

The equilibrium Josephson current $J(\phi)$ flowing through the phase-biased molecular junction is given by

$$J(\phi) = \frac{2e}{\hbar}\,\partial_\phi F \ , \tag{4.2}$$

where ϕ is the superconducting phase difference and $F = -T \ln Z$ is the free energy (T is temperature). Following the standard procedure, we calculate the partition function Z by using an imaginary time path-integral approach to trace out electronic degrees of freedom. As a result, the free energy can be written as (we set $\hbar = e = 1$):

$$F = -T \sum_{\omega_n} \ln \det M_{\omega_n} \ , \tag{4.3}$$

where the sum runs over fermionic Matsubara frequencies, and (assuming symmetric tunneling coupling to the leads, $\Gamma_{L,R} = \Gamma/2$)

$$M_\omega = -i\omega + \epsilon\sigma_z + JS + \frac{\Gamma}{\sqrt{\Delta^2 - (i\omega)^2}}\,[-i\omega + \Delta\cos(\phi/2)\,\sigma_x] \ . \tag{4.4}$$

The Andreev level spectrum is determined by the dispersion equation (for real variable z) $\det M_{iz} = 0$. We have found that this equation has always two roots $z = E_{1,2}$ lying within the subgap region $[-\Delta\,,\,\Delta]$. There are thus always two Andreev bound states, as in the zero spin case: the effect of the spin term is merely to move these two states, but it does not introduce new bound states.

From Eqs. (4.2) and (4.3), one can calculate the total Josephson current by summing over the Matsubara frequencies:

$$J(\phi) = -T \sum_{\omega_n} f(\omega_n) \ , \quad f(\omega) = 2\,\frac{\partial_\phi \det M_\omega}{\det M_\omega} \ . \tag{4.5}$$

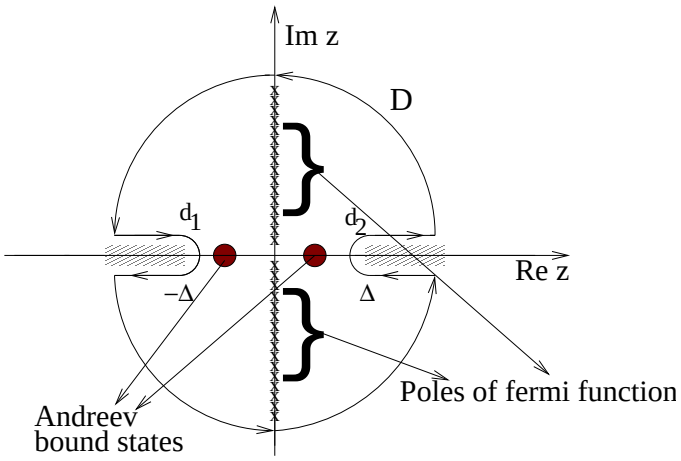

Figure 4.2: The contour C includes the poles of the Fermi function, two Andreev bound states and the contribution from the branch cuts.

However, for physical interpretation, it is convenient to separate explicitly the contributions of the Andreev bound states and of the continuum. In order to calculate these contributions, we take advantage of the fact that the Matsubara frequencies are the poles of the Fermi function $n_F(z) = \left(e^{z/T}+1\right)^{-1}$. From evaluating the contour integral $I = \int_C (dz/2\pi i)\, f(z) n_F(z)$, see Fig. 4.2, we can present the Josephson current as a sum of two terms:

$$J = I_b + I_c \ , \tag{4.6}$$

$$I_b = -n_F(E_1)\, \mathrm{res} f(E_1) - n_F(E_2)\, \mathrm{res} f(E_2) \ , \tag{4.7}$$

$$I_c = \frac{1}{\pi}\left[\int_{-\infty}^{-\Delta} + \int_{\Delta}^{\infty}\right] dz\ \mathrm{Im}\left\{f(z+i0)\, n_F(z+i0)\right\} \ , \tag{4.8}$$

where I_b is a sum over the discrete subgap spectrum (Andreev levels) and I_c is an integral over the continuous spectrum. As we see from Eq. (4.7), the contribution from each Andreev bound state is proportional to the occupation number $n_F(E_i)$ of this level ($i = 1, 2$).

Mechanism of the π-shift

In Fig. 4.3, we plot the Josephson current $J(\phi)$ for different values of the spin coupling $s = JS/\Delta$. With increasing the strength of the spin coupling, the Josephson current exhibits an anomalous phase dependence. We clearly see a π-junction type behavior as the magnitude of the spin coupling reaches some critical value s_c (depending on the interface transparency Γ) which results in a reversal of the Josephson current. In Fig. 4.4, we plot the free energy F as a function of the phase difference ϕ. We see that with increase of the spin coupling strength the transition from the 0 to the π phase is clearly marked by the shift of the global

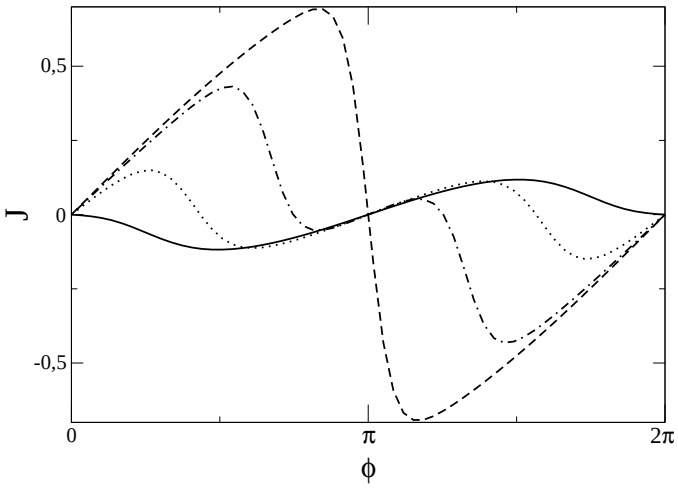

Figure 4.3: Josephson current J in units of $e\Delta/\hbar$ for $s = 0$ (dashed line), 2 (dash-dotted line), 3.3 (dotted line), and 4.2 (full line). In all cases we take $\Gamma = 4\Delta$, $\epsilon = 0$, and $T = 0.05\Delta$. The π junction behavior is clearly seen with increasing magnetization.

minimum of F from $\phi = 0$ to $\phi = \pi$ leading to a negative Josephson coupling. In Fig. 4.4, the labeling of the respective junctions as $0, 0', \pi'$ and π configurations follows from the respective stability of $\phi = 0$ and $\phi = \pi$ configurations. For a $0(\pi)$ junction, only $\phi = 0(\phi = \pi)$ is a stable minimum of $F(\phi)$. For the other two intermediate cases, both $\phi = 0$, π are local minima and depending on whether $\phi = 0\,(\phi = \pi)$ is the global minimum, one has a $0'\,(\pi')$ junction. Of particular interest is the bistable configuration, in which both the minima (at $\phi = 0$ and $\phi = \pi$) are degenerate. This feature can be effectively exploited to design a qubit, where the two phase states of the Josephson junction represent the qubit states.

The ability to distinguish, in the Josephson current, between the contributions from each Andreev bound state and from the continuum provides us with a simple picture for the mechanism leading to the π-shift in the presence of large spin coupling. The origin of the continuum current is due to the phase difference between the two superconductors, which breaks the symmetry between the left and right-moving quasiparticles. Besides, the continuum current generally flows opposite to the bound state current [53, 55]. Thus, because the effect of the spin coupling is to reduce the Andreev bound states contribution, this gives more importance to the continuum contribution, and leads to the π-shift when the continuum current dominates.

A remarkable feature of our system is that the π-shift behavior can be controlled and reversed using the different parameters of the system. This is important for potential experimental implementations, as some of these parameters can be accessed relatively easily (one can, for example, move the dot level by using a gate voltage), contrary to the spin coupling which is a fixed quantity. Our results show that, when the spin coupling is large enough to have a π junction, a change

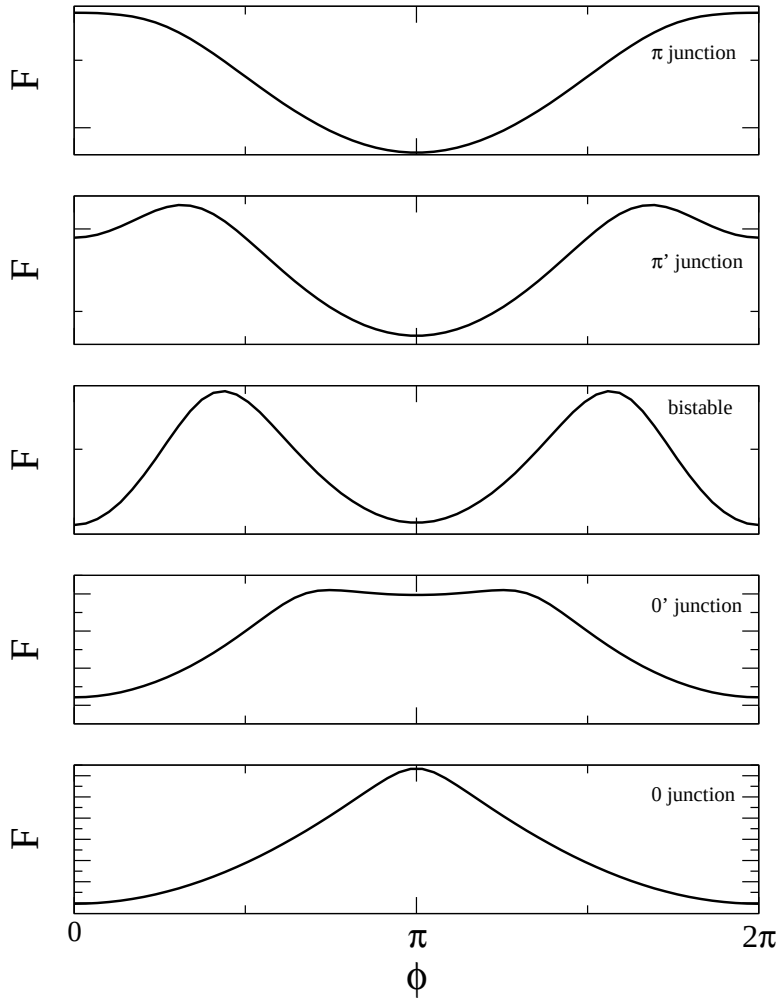

Figure 4.4: Free energy F (in arbitrary units) as function of the phase difference (ϕ) for increasing spin (from bottom to top): $s = \{0, 2, 3.3, 3.7, 4.2\}$. The other parameters are the same as in Fig. 4.3.

in any of the parameter of the system (dot level position ϵ, coupling to the leads Γ, and asymmetry of this coupling) makes it possible to have the system behave as a standard 0 junction going through any intermediate situation between π and 0 junction.

In view of an experimental realization, one must ask if the strength of the spin coupling within a given molecular magnet is large enough to observe the π junction behavior. A gross estimate can be obtained by calculating the interaction energy of two magnetic dipoles at a distance which is of the molecule size. Taking a spin $S = 10$ for the molecule (as in $Mn_{12}Ac$), and a distance ~ 5 Å, we find the interaction energy ~ 0.1 meV, which is of the same order as the superconducting gap. This estimate shows that the π junction regime due to spin coupling may be reached experimentally.

4.2 JOSEPHSON CURRENT THROUGH A QUANTUM DOT WITH SPIN-ORBIT COUPLING

The effects of spin-orbit coupling on transport phenomena in quantum dots have been studied extensively in recent years because of their potential for future electronic devices, mainly for quantum information and spintronics applications. Many of these devices rely on the Rashba spin-orbit interaction effect [56] which originates from an intrinsic macroscopic electric field in a semiconductor quantum well with anisotropic confinement. Coupling the spin degree of freedom of an electron to its orbital motion gives a useful handle for manipulating and controlling the electron spin by means of a gate electrode or external electric/magnetic fields. The pioneering spin-transistor proposal of Datta and Das [57] best exemplifies the relevance of spin modulating charge flow in a semiconductor with ferromagnetic leads. There have also been many other works on related topics where the spin-orbit interaction plays a central role.

Despite the large recent interest concerning spin-orbit effects in quantum dots, the question of how the Josephson current is modified by spin-orbit couplings has barely been addressed. In paper VII, we reconsider the theory of the Josephson effect through a quantum dot in a two-dimensional electron gas (2DEG), taking into account Rashba and/or Dresselhaus spin-orbit couplings.

2DEG devices based on InAs-related materials are known to exhibit strong gate-tunable [58] Rashba (and possibly Dresselhaus) spin-orbit couplings. Supercurrents through related devices have been probed by several experiments [59, 60, 61]. It is thus not only of academic interest to quantitatively examine the effects of Rashba/Dresselhaus spin-orbit couplings on the equilibrium Josephson current. Moreover, very recently, gate-tunable supercurrents through thin InAs nanowires have been reported [62, 63], revealing complex current-phase relations such as π-junction behavior. Although we study a 2DEG geometry, our results are also relevant for such nanowires: the transport channels reside in a surface charge layer, and Rashba terms due to narrow-gap and strong confinement fields

dominate over all other SO couplings. In those experiments, Josephson currents through few-level dots have already been achieved.

Model and formulation

We consider a (multi-level) quantum dot formed by a confinement potential $V(\mathbf{r})$ within a 2DEG determined by the layer sequence of a semiconductor heterostructure; the growth direction is taken to be along the z direction. The single-particle Hamiltonian of electrons confined to the dot is the sum of free-electron dispersion term and the potential V (we put $\hbar = 1$):

$$h_{QD}(\mathbf{r}) = \frac{(-i\nabla + \mathbf{a})^2 - 2\alpha^2}{2m} + \mathbf{b}\cdot\vec{\sigma} + V(\mathbf{r}) \ , \tag{4.9}$$

where $\mathbf{r} = (x, y)$, $\mathbf{b} = (b_x, b_y, b_z)$ is a constant external Zeeman field (including gyromagnetic and Bohr magneton factors), and $\vec{\sigma} = (\sigma_x, \sigma_y, \sigma_z)$ with standard Pauli matrices $\sigma_{x,y,z}$. Orbital magnetic fields could also be taken into account in our model but give no qualitative changes. In Eq. (4.9), the $x(y)$ component of the operator $\mathbf{a} = (a_x, a_y)$ acts in spin space,

$$\mathbf{a} = \alpha \Big(\ \sin\theta \ \sigma_x - \cos\theta \ \sigma_y \, , \quad \cos\theta \ \sigma_x - \sin\theta \ \sigma_y \ \Big) \ , \tag{4.10}$$

and contains the combined effect of Rashba (α_R) and linear Dresselhaus (α_D) couplings via

$$\alpha = \sqrt{\alpha_R^2 + \alpha_D^2}, \quad \sin\theta = \alpha_D/\alpha \ . \tag{4.11}$$

These two are generally the most important spin-orbit couplings in quantum dots based on 2DEG geometries.

The quantum dot is coupled via tunneling to two 3D superconducting electrodes (assuming the same BCS gap Δ on both banks). Although the connection between the superconducting leads and the dot is taken in the form of a tunneling Hamiltonian (like in the previous section), we treat these terms to all orders, and this provides justification for ignoring Coulomb interactions on the quantum dot. Over the last decade, several works [64, 65, 66] have shown that in the limit of high transparency, i.e., for tunneling rates Γ large compared to the dot charging energy, charge quantization (Coulomb blockade) effects are strongly suppressed due to large charge fluctuations. The high transparency limit is in fact quite relevant in the light of recent experiments where quantum dots are embedded in a Josephson setting using InAs nanowires [62, 63]. Note also that an observable Josephson current usually requires high-transparency contacts.

To calculate the equilibrium Josephson current (4.2), we adopt a functional-integral representation of the partition function Z, which here requires a slightly nonstandard formulation due to the spin-flip terms caused by the spin-orbit processes. The presence of spin flip processes makes it necessary to introduce two types of Nambu spinors in order to trace out the electronic degrees of freedom. In

our approach, this doubling of spinor space is accompanied by the corresponding reduction of energy space (restricted to positive Matsubara frequencies), so in the end it does not create a double-counting problem.

Given the fact that the model Hamiltonian is quadratic in the fermion variables, we have derived the equilibrium Josephson current-phase relation, which does not involve approximations and contains contributions of the Andreev bound states and of the continuum. The calculation of the Josephson current requires only a simple numerical routine and allows for a quantitative comparison to experimental data.

Spin-orbit induced oscillations of the critical current

In order to get insight into the relevant physics, we consider the simplest cases of a single and of two spin-degenerate quantum dot levels. They are derived for $V(\mathbf{r})$ given as hard-box confinement along the x-axis, $-L/2 \leq x \leq L/2$, plus a harmonic transverse confinement of frequency scale $\omega_\perp$. The level index $n = (n_x, n_y)$ then contains the respective integer quantum numbers $n_x \geq 1$ and $n_y \geq 0$, with eigenenergy (up to an additive constant related to a gate voltage)

$$\epsilon_n = \frac{(\pi n_x/L)^2}{2m} + \omega_\perp(n_y + 1/2) \ . \tag{4.12}$$

In the *single level* case, spin orbit couplings do not affect the Josephson current in the absence of Zeeman field $\mathbf{b}$ [67]. Spin-orbit effects can only enter via the effective magnetic field $\mathbf{B}$ given by

$$B = \left[(b_x \sin\theta - b_y \cos\theta)^2 + F_{n_x}\left(b_z^2 + (b_x\cos\theta + b_y \sin\theta)^2\right)\right]^{1/2}, \tag{4.13}$$

where F_n depends on the distance L between the leads contacts,

$$F_n(\alpha L) = \left(\frac{\sin(\alpha L)}{\alpha L(1-(\alpha L/\pi n)^2)}\right)^2 \ . \tag{4.14}$$

For $b_x = b_y = 0$, the oscillatory behavior of B due to the dependence of F_n on the spin precession phase αL is most pronounced, with $B = 0$ for $\alpha L = 2\pi k$ (integer k). This oscillation may then persist in the Josephson current, suggesting the appearance of Datta-Das like oscillations in the critical current. These oscillations are displayed in Fig. 4.5; for $n_x = 1$, such oscillations are not yet observable, but they become visible for $n_x > 1$. For $\Gamma \gg \Delta, |\mathbf{b}|$, the amplitude of the current oscillations is of the order of $(e\Delta/\hbar)(|\mathbf{b}|/\Gamma)^2$. The oscillation period in the critical current is roughly set by $\alpha L = \pi$, similar to the normal-state case of the Datta-Das transistor [57]. Moreover, by systematic variation of the magnetic field ($\mathbf{b}$) direction within the x-y plane, one could measure the spin-orbit angle θ from the Josephson current.

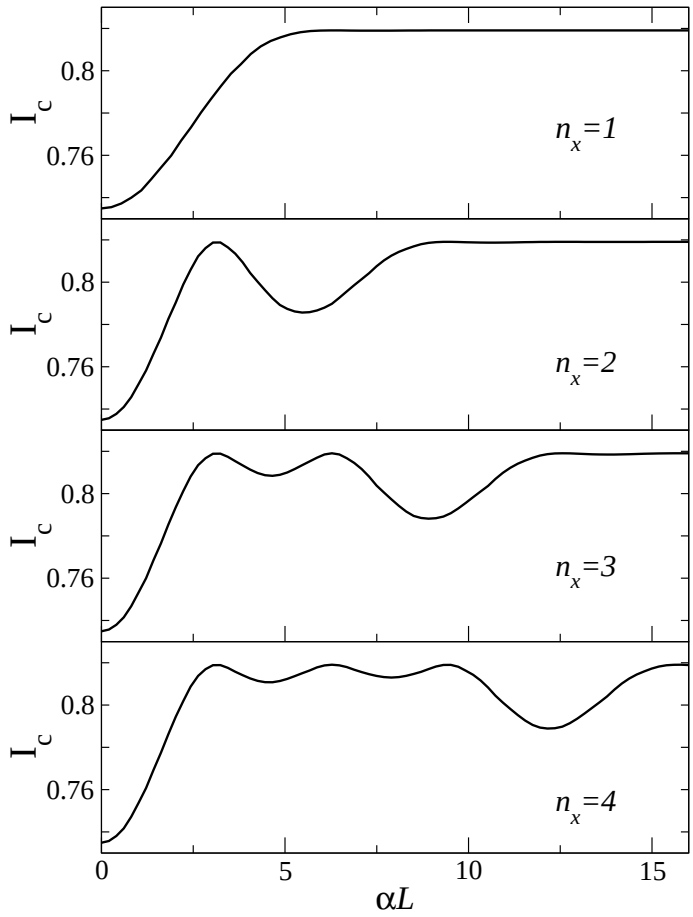

Figure 4.5: Spin-orbit induced oscillations of the critical current I_c (in units of $e\Delta/\hbar$) in a single-level dot as a function of αL for $\mathbf{b} = (0, 0, 0.2\Gamma)^T, \Gamma = 10\Delta, T = 0.05\Delta$. The dot is taken in the transverse ground state $n_y = 0$, with only one resonant level $\epsilon_{n_x} = 0$, for various n_x.

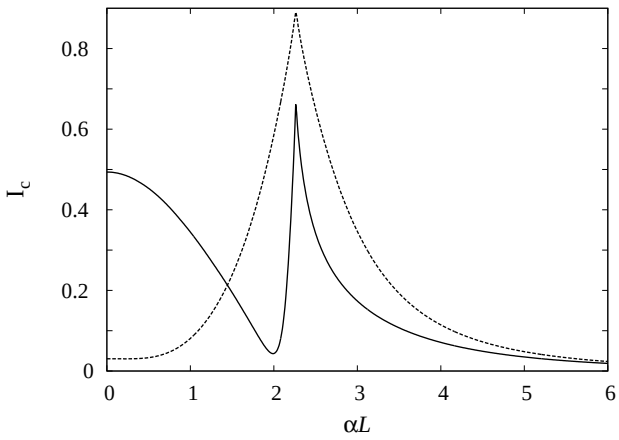

Figure 4.6: Zero-field critical current as a function of α in a two-level quantum dot. We take $\epsilon_0 = 0$, $\omega_\perp = 20$ meV, $\theta = 0$, $\Delta = 1$ meV, $L = 20$ nm, $m = 0.035m_e$, and $T = 0.01\Delta$. (These values are appropriate for Nb contacts.) Results are shown for two cases (where $\Gamma_{12} = \sqrt{\Gamma_{11}\Gamma_{22}}$), namely either $\Gamma_{11} = 20\Delta$ and $\Gamma_{22} = 0$ (only one level couples to the leads, solid line) or $\Gamma_{22} = \Gamma_{11} = 10\Delta$ ('democratic tunneling', dashed line).

Two-level dot

A quantum dot with *two levels* is a minimal model which allows us to get spin-orbit related effects on the Josephson current without a magnetic field, $\mathbf{b} = 0$. As a concrete example, we consider the dot states given by the first two oscillator eigenstates ($n_y = 0, 1$) in the longitudinal ground state ($n_x = 1$).

Figure 4.6 shows typical numerical results for the critical current I_c as a function of α for two choices of the hybridization parameters Γ_{nn} characterizing the level-lead coupling. The shown range for αL can be realized in InAs-based devices [58], and thus the supercurrent can be strongly modified by experimentally relevant spin-orbit couplings in multi-level quantum dots, with pronounced minima or maxima in I_c. The apparent cusp-like maximum in Fig. 4.6 is smooth and does not represent singular behavior.

Note that the results displayed in Fig. 4.6 are for large Γ/Δ, where the Josephson current is predominantly carried by the Andreev bound state contribution $I_A(\phi)$. The latter can be analytically evaluated, and (at $T = 0$) is expressed in terms of an effective transmission probability $\mathcal{T}_0$,

$$I_A(\phi) = \frac{e\Delta}{2\hbar} \frac{\mathcal{T}_0 \sin\phi}{\sqrt{1 - \mathcal{T}_0 \sin^2(\phi/2)}} \ . \tag{4.15}$$

The minimum in I_c is thus expected when $\mathcal{T}_0 \simeq 0$, in accordance with the values seen in Fig. 4.6. On the other hand, the maximum in I_c (where I_c may exceed the $\alpha = 0$ value) is found for $\mathcal{T}_0 = 1$, again explaining the numerical result in Fig. 4.6.

The resonance behavior of the Josephson current stems from the interplay between spin-orbit couplings and the multilevel nature of the quantum dot. A qualitative argument in favor of such a resonance process can be reached as follows. Schematically, when a Cooper pair enters the dot from the left, either its electrons occupy the same transverse level or they can choose different 'paths' (different transverse levels), in a manner quite similar to a cross-Andreev scattering process [68, 69]. The spin-orbit interaction acts differently in these two levels because the longitudinal momenta of both states are not identical. Two electrons entering the quantum dot from, say, the left electrode have initially antiparallel spins, but their respective spins now precess at different rates because of this mismatch in longitudinal momentum. Depending on the value of αL, the two electrons which then exit the quantum dot at the right side may, however, be brought back to an antiparallel configuration, leading to a resonance in the critical current caused by the presence of spin-orbit couplings. On the other hand, if the spins do not reach the antiparallel configuration, the Josephson current will be reduced.

More than one resonance can be achieved by a careful choice of parameters. This effect is illustrated in Fig. 4.7. For a multilevel dot with small confinement

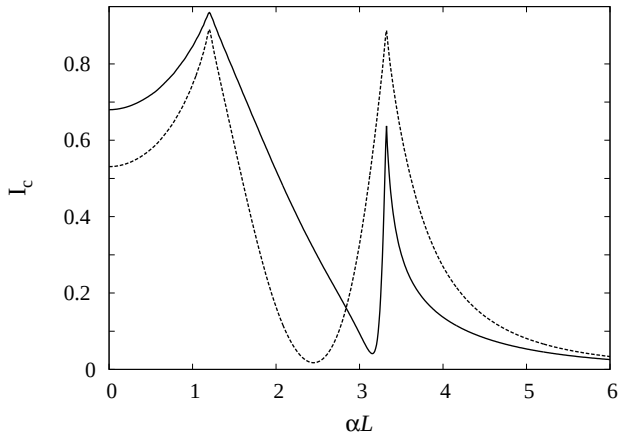

Figure 4.7: Same as Fig. 4.6, but for $\epsilon_0 = 15$ meV.

frequency, the multiple resonances associated with all possible pairs of paths (pairs of levels) will start to overlap significantly. It is then natural to expect that in the limit of very wide quantum dots, these averaging effects will wash out any spin-orbit related structures in the Josephson current, consistent with the results of Ref. [70] for infinite width.

CHAPTER 5

PHONON-INDUCED DECOHERENCE OF ANDREEV LEVEL QUBIT

Implementation of Josephson junctions for quantum computation is an interesting theoretical problem and a great challenge for experiment. Several realizations of a superconducting qubit have been proposed based on the operation either with phase (flux) or/and charge (for review, see [71, 72]). In all these realizations of a superconducting qubit, the quantum fluctuations of charge and phase play the central role, while the Josephson junction is assumed to be a macroscopic object which does not exhibit any quantum fluctuations. In paper I we have proposed a *new type* of superconducting qubit, the so-called Andreev level (AL) qubit, which is based on quantum fluctuations of the current in a quantum point contact embedded in a superconducting loop. In the AL qubit, the switching between the two persistent current states in the loop is achieved by employing a true microscopic system formed by the two-level Andreev bound state system.

The AL qubit operation frequency must significantly exceed the relaxation and dephasing rates of Andreev levels. Even if good decoupling of the qubit states from the continuum quasiparticle states is achieved, there are still soft microscopic modes in the junction which could couple to the Andreev levels. These modes present a potential source of "intrinsic" decoherence of the AL qubit, in addition to the commonly discussed external decoherence (due to bias fluctuations, radiation, etc.). In paper II, we have considered such an intrinsic decoherence of the AL qubit related to acoustic phonons. Investigation of this problem has shown that the interaction of Andreev levels with phonons does not impose any further limitations on the functioning of AL qubit.

5.1 DYNAMICS OF ANDREEV LEVEL QUBIT

It is theoretically well established [73, 74] and convincingly confirmed by experiments on atomic-size contacts [75, 76, 77] that the Josephson current through a superconducting quantum point contact (QPC) is primarily carried by Andreev bound states. The Andreev level wave functions are localized in the vicinity of the contact over a distance of the order of the superconducting coherence length,

and the number of Andreev bound levels is limited to one pair of levels per conducting electronic mode. Thus, a superconducting QPC may be viewed as a kind of quantum dot which contains a finite number of localized quantum states.

In a single-channel QPC, the pair of Andreev bound states spans the Hilbert space of the qubit. In a perfectly transparent QPC (no electron backscattering), the Andreev bound states are simultaneously eigenstates of the current operator, and carry well defined currents flowing through the contact in the opposite directions. In QPCs with finite reflectivity, $R = 1 - D \neq 0$, these current states undergo hybridization, which leads to opening of a gap in the Andreev level spectrum (see Fig. 5.1),

$$E_a(\phi) = \Delta\left[1 - D\sin^2(\phi/2)\right]^{1/2} , \tag{5.1}$$

where ϕ is the superconducting phase difference across the contact, and Δ is the BCS gap. In this case, the current undergoes strong quantum fluctuations

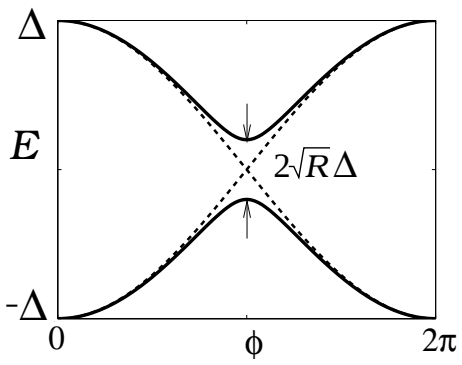

Figure 5.1: Spectrum of the Andreev levels in a QPC with finite reflectivity ($R = 0.04$) (solid line), the level anticrossing is produced by electronic back scattering; at $R = 0$ the Andreev levels (dashed line) coincide with the current eigenstates.

because the qubit eigenstates are superpositions of the current states.

The most important requirement for the operation of AL qubit is small reflectivity of the QPC, $R \ll 1$. In a highly transmissive contact biased at ϕ close to π, the Andreev levels lie deep within the superconducting gap, which makes them well decoupled from the continuum quasiparticle states during the qubit evolution. Besides, in the case of small R, the critical Josephson current approaches the upper bound for supercurrent per conducting mode, $I_c \approx e\Delta/\hbar$ (0.37 μA for Nb), and the Josephson energy is close to the gap value, $E_J \approx \Delta$. In experimental atomic-size QPCs, reflectivities as small as $R \sim 0.01$ have been detected [77].

Coherent coupling of the Andreev levels to the supercurrent flowing through the contact makes the Andreev levels accessible for manipulations and for measurements. This is achieved by embedding the QPC in a superconducting loop forming an rf SQUID (see Fig. 5.1). By ramping the external flux or by applying

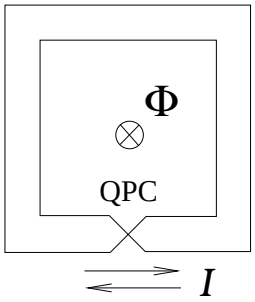

Figure 5.2: Sketch of the Andreev level qubit: a low inductance superconducting loop with a quantum point contact (QPC). Φ is the magnetic flux; the arrows indicate fluctuating persistent currents.

properly designed rf flux pulses, one can drive Andreev levels from the ground state to an excited state, and then this state can be measured by monitoring the induced flux, similar to the flux qubits. The induced flux through the SQUID, however, undergoes strong quantum fluctuations even in the ground state: the superposition of clockwise and counter-clockwise persistent current states generates the superposition of the flux states of the SQUID. Note that hybridization of the flux states in the AL qubit loop is produced by the microscopic processes of electronic back scattering in the QPC. This is different from the macroscopic superconducting flux qubits [78, 79, 80] and charge-phase qubit [81], where the hybridization is provided by charge fluctuations on the tunnel junction capacitors.

Using a path integral approach, we have derived an effective Hamiltonian describing Andreev levels coupled to flux (phase) fluctuations. The central technical difficulty here was to extend the theory, originally developed for tunnel junctions, to the interesting case of *high transmission* QPCs. This problem has been overcome by incorporating the exact boundary condition in the QPC action. The derivation involves integration over electronic degrees of freedom in the superconducting electrodes, and the result is valid for Andreev levels with low energies. Assuming that the phase dynamics is slow on the time scale of $\hbar/\Delta$, the effective Hamiltonian for the two-level Andreev system is given by

$$H = \Delta\, e^{-i\sigma_x\sqrt{R}\,\phi/2}\left(\cos\frac{\phi}{2}\,\sigma_z + \sqrt{R}\,\sin\frac{\phi}{2}\,\sigma_y\right) + H_{osc}[\phi]\ , \tag{5.2}$$

where H_{osc} describes an LC oscillator formed by the junction capacitance C and the superconducting loop inductance L.

The phase dynamics is strongly coupled to the Andreev levels. And this is a vital part of the ALQ operation. The Andreev levels could not be manipulated if the phase dynamics was frozen because, first, any manipulation requires variation of the current, and secondly, the read out of the Andreev levels can only be performed via measuring the quantum state of the loop oscillator. An obvious

way to solve this problem and preserve the qubit property of the coupled system is to "enslave" the loop oscillator by choosing the oscillator level spacing $\hbar\omega_p$ (ω_p is a plasma frequency of the superconducting loop) much larger than the Andreev level spacing, $\hbar\omega_p \gg 2E_a$. Then the Andreev state evolution will not excite the oscillator, which will remain in the ground state and adiabatically follow the evolution of the Andreev levels. Averaging out the ground state phase fluctuations around the bias value ϕ_b results in an effective qubit Hamiltonian:

$$h_a = \Delta \left(\cos\frac{\phi_b}{2}\,\sigma_z + \sqrt{R^*}\sin\frac{\phi_b}{2}\,\sigma_y \right) , \tag{5.3}$$

where $R^* = e^{-\lambda} R$ is the reflectivity of the contact renormalized by the Franck-Condon suppression factor. This renormalization effect can be understood as the effect of inertia of the loop oscillator, which works against the effect of electronic back scattering. Because of renormalization of the contact reflectivity, the AL spectrum is modified, $E_a \to E_a^*$, and the qubit frequency reduces. This might be important for practical applications to tune the qubit frequency by choosing the circuit parameters.

The Andreev level dynamics is described by a Liouville equation,

$$i\hbar\partial_t \rho_a = [h_a\,,\rho_a] \ . \tag{5.4}$$

In equilibrium, the qubit density matrix ρ_a is diagonal in the Andreev level eigenbasis, and the matrix elements are determined by the Fermi factors $f(\pm E_a^*)$. This is the initial condition for the qubit operation. Since the sum of the level populations $f(E_a^*) + f(-E_a^*) = 1$ is preserved during the time evolution, the density matrix satisfies the normalization condition $\mathrm{tr}\,\rho_a(t) = 1$. For a QPC with reflectivity $R \sim 0.01$, the Andreev level energy $\sim \sqrt{R}\Delta$ corresponds to a frequency of the order or larger than 10 GHz, which considerably exceeds typical experimental temperatures (below 100 mK). Thus, the AL qubit should exhibit well pronounced spin 1/2 quantum dynamics, which is the basis for the qubit application.

5.2 ANDREEV LEVEL–PHONON INTERACTION

Qubit decoherence is usually described through collision terms in the Liouville equation for the qubit density matrix taking into account the interaction with an environment. In paper II we have derived the phonon-induced collision terms in the equation (5.4) for AL qubit density matrix, and evaluated the decoherence of the AL qubit.

While the description of free qubit evolution is possible in the terms of the single-particle density matrix, evaluation of the collision terms goes beyond the single-particle approximation and requires the knowledge of *electronic two-particle correlation* functions. This is because the Andreev levels do not form a rigorously isolated system but rather belong to a large fermionic system of the superconducting electrons in the contact electrodes. To derive the collision terms, we have

appled the nonequilibrium Keldysh Green function technique combined with the path integral approach. This method takes into account many-body effects in the form of the Pauli exclusion principle, leading to a non-linear form of the collision terms and eventually to the suppression of decoherence.

Kinetic equation

As an intrinsic source of decoherence of the Andreev levels, we consider only longitudinal acoustic phonons propagating in the bulk electrodes, and describe the electron-phonon interaction within the deformation potential approximation. By integrating out the bulk degrees of freedom (including phonons), and using perturbation theory expansion in the weak electron-phonon coupling, we have derived the saddle-point Dyson equation for the Keldysh Green function of Andreev levels, which leads to a kinetic equation for the qubit density matrix ρ. The equations for the diagonal $\rho_z = (\rho_{11} - \rho_{22})/2$ and off-diagonal ρ_{12} component of the density matrix are given by (in the interaction picture)

$$\partial_t \rho_z = -\nu \Big[\, (2N+1)\, \rho_z \, (1-\rho_z) - 1/4 \Big] \, , \tag{5.5}$$

$$\partial_t \rho_{12} = -\nu \, \left(N + 1/2 - \rho_z\right) \rho_{12} \, , \tag{5.6}$$

where ν is the phonon-induced transition rate between the qubit levels, and $2N + 1 = \coth \beta E_a^*$ (β is inverse temperature). It is important to mention that the derived effective AL–phonon interaction has purely transverse origin, i.e., while inducing interlevel transitions and hence the relaxation, it does not produce any additional dephasing to the one associated with the relaxation.

Eqs. (5.5) (5.6) are drastically different from the linear Bloch-Redfield equation describing decoherence of the macroscopic superconducting qubits, and have qualitatively different solutions, as illustrated in Fig. 5.3. The time evolution of the diagonal (relaxation) and off-diagonal (dephasing) parts of the density matrix is determined by the decoherence rate $\Gamma = \nu / \sinh(\beta E_a^*)$. However, at low temperature $\beta E_a^* \gg 1$, Γ becomes exponentially small. As a result, there is a wide time interval, $t < 1/\Gamma$, where both the relaxation and dephasing follow the power law ($\delta\rho_z(t)$ is the deviation from equilibrium),

$$\delta\rho_z(t) \quad , \quad \tilde{\rho}_{12}(t) \propto \frac{1}{\nu t} \, , \tag{5.7}$$

and only at very large times, $t \gg 1/\Gamma$, the decoherence undergoes a crossover to an exponential regime. The power-low decay of the AL density matrix reflects the fermionic nature of the Andreev states and leads to considerable enhancement of the decoherence time at low temperature. We note that the exponentially small relaxation rate is known for the quasiparticle recombination in bulk superconductors [82].

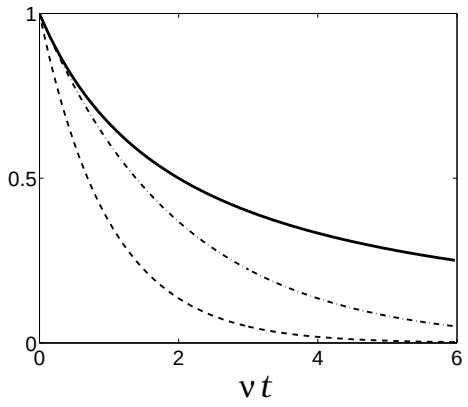

Figure 5.3: Decay with time of a "cat" state (at $t = 0$ $\delta\rho_z = \rho_{12} = 1/2$). Bold line indicates the evolution of normalized density matrix elements for AL qubit; $1/\beta = 0.2E_a^*$. For comparison, exponential relaxation and dephasing of a macroscopic superconducting qubit are illustrated with the dashed and dash-dotted lines, respectively.

Phonon–induced transition rate

To evaluate the phonon-induced transition rate between the Andreev levels, one needs to specify the geometry of the junction in greater detail. In paper II, we model the contact with a smooth on the Fermi wave length scale (adiabatic) constriction which is formed by a hard-wall potential and has an axial symmetry

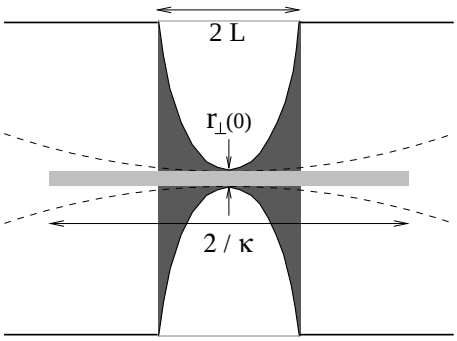

Figure 5.4: Interaction region of the Andreev levels with phonons in short QPC (dark shadow) and in long QPC (light shadow); in long QPC, increase of the constriction radius (dashed line) can be neglected.

(see Fig. 5.4). The length L of the constriction is assumed to be small on the scale of the superconducting coherence length ξ_0. The magnitude of the transition rate essentially depends on the parameter $r_\perp Q$, where $r_\perp$ is the radius of the neck of the constriction, and Q is the wave vector of phonons responsible for the interlevel transitions. For atomic-size constrictions, this parameter is small, $r_\perp Q \ll 1$, and

the relevant phonon wave length is typically small compared to the penetration length of the Andreev level wave function into the bulk electrodes. The rough estimation, assuming $r_\perp = \text{const}$, shows that the transition rate is given by

$$\nu_0 \sim \sqrt{R^*}\, \tau_{ph}^{-1}(E_a^*) \ , \tag{5.8}$$

where $\tau_{ph}^{-1}(E_a^*) \sim E_a^{*3}/\hbar\Theta_D^2$ is a bulk electron-phonon relaxation rate evaluated at the Andreev level energy (Θ_D is the Debye temperature). Thus, in highly transmissive QPCs with $R^* \ll 1$, the phonon-induced transition rate between the AL levels is significantly reduced compared to the transition rate for the bulk quasiparticles. We note that ν_0 is proportional to $\sqrt{R^*}$, and it turns to zero in the case of perfectly transparent constriction. This stems from the fact that the relevant phonons have small wave vectors $Q \ll k_F$ and are not able to provide large momentum transfer ($\sim 2k_F$) during scattering with electrons.

Eq. (5.8) can be qualitatively applied to long constrictions, whose length exceeds the coherence length ξ_0. However, for short constrictions considered here, the effect of rapid spreading out of the Andreev level wave function is essential, and the approximation $r_\perp = \text{const}$ is not appropriate. As follows from our analysis, in short constrictions the transition rate is even more reduced,

$$\nu \sim (L/\xi_0)\ \nu_0 \ , \tag{5.9}$$

which is owing to the small spatial region available for the Andreev level-phonon interaction. For $R^* < 0.01$ the transition rate is smaller than the qubit operation frequency by at least a factor of 10^5.

CHAPTER 6

DETECTION OF CURRENT MOMENTS WITH A DISSIPATIVE RESONANT CIRCUIT

The knowledge of all current moments, at arbitrary frequencies, allows to characterize completely the statistics of electron transfer in mesoscopic devices. "Zero" frequency noise measurements have provided valuable diagnosis for transport in the past (in particular, providing information about the effective charge of carriers and their statistics). The third (and fourth) current moments have recently been measured experimentally for a few specific systems [83, 84, 85] at low frequencies. Yet, current moments at high frequencies are difficult to measure, and typically require an on-chip measuring apparatus [86, 87, 88, 89, 90, 91]. High frequency noise detection provides information which is not apparent at zero frequency (for instance, when characterizing excitations in carbon nanotubes [92, 93]), and is inevitably influenced by the electromagnetic environment surrounding the device to be measured. In paper IX, we present a scheme for the measurement of the noise and third moment at high frequencies, using a resonant circuit as a detector. A central issue deals with the role of the electromagnetic environment on the measurement, which has been discussed in different contexts [94, 95, 96, 97, 98].

On-chip noise measuring proposals are either based on capacitive coupling, on inductive coupling, or both [99]. Any measurement involves the filtering of frequencies by the detection circuit, with an appropriate bandwidth: this justifies the choice of a generic resonant circuit. A dissipationless LC circuit was proposed [86] to measure high frequency noise. The measured noise (the squared charge fluctuations on the capacitor) is then a combination of the unsymmetrized current correlators. The charge fluctuations are inversely proportional to the adiabatic switching parameter used for the coupling. This parameter has thus to be interpreted as a line width which should be computed from the first principles. In the same spirit, the radiation line width of a Josephson junction was shown to originate from the voltage fluctuations of the external circuit [100]. A fundamental question here is to derive this line width and therefore to see how dissipation affects the measurement of the higher current moments.

6.1 GENERATING FUNCTIONAL APPROACH

The setup is depicted in the upper part of Fig. 6.1a: a lead from the mesoscopic device is inductively coupled to a resonant circuit (capacitance C, inductance L, and dissipative component R). Repeated time measurements are operated on the charge q, leading to an histogram which is qualitatively depicted in Fig. 6.1a: a reference histogram is made for zero voltage (left), yielding the zero bias peak position, its width, skewness, etc. In the presence of bias, this histogram is shifted (right), and it acquires a new width. Information about all current moments at high frequencies is coded in such histograms. The basic Hamiltonian which describes the dissipative oscillator circuit reads: $H = H_0 + V$, where $H_0 = H_{LC} + H_{env}$ is the Hamiltonian of the uncoupled system "LC oscillator plus environment", and V describes the coupling. Below we use a path integral formulation to describe the evolution of the system. In the absence of dissipation and coupling to the mesoscopic device, the Keldysh action describing the charge of the LC circuit reads:

$$S_{LC}[q] = \frac{1}{2}\int dt dt' \mathbf{q}^T(t) G_0^{-1}(t-t')\sigma_z \mathbf{q}(t') \ , \tag{6.1}$$

where $G_0^{-1}(t-t') = M[(i\partial_t)^2 - \Omega^2]\delta(t-t')$, is the (inverse) Green function of an harmonic oscillator of mass $M \equiv L$, $\Omega = (LC)^{-1/2}$ is the resonant frequency of the circuit, $\mathbf{q}^T = (q^+, q^-)$ is a two component vector which contains the oscillator coordinate on the forward/backward contour, and σ_z is a Pauli matrix in Keldysh space. Dissipative effects are treated within the Caldeira-Leggett model [101], where the environment is modeled by a set of harmonic oscillators (bath) with frequencies $\{\omega_n\}$; the coordinate q is coupled linearly to the bath oscillators, $V = q\sum_n \lambda_n x_n$, with the coupling constants λ_n. The partition function of the LC oscillator plus bath, $Z = \int \mathcal{D}q\mathcal{D}x e^{iS[q,x]}$, has an action:

$$S = S_{LC} + \frac{1}{2}\sum_n \mathbf{x}_n^T \circ D_n^{-1} \circ \sigma_z \mathbf{x}_n - \mathbf{q}^T \circ \sigma_z \sum_n \lambda_n \mathbf{x}_n \ , \tag{6.2}$$

where $D_n^{-1}(t) = M_n[(i\partial_t)^2 - \omega_n^2]\,\delta(t)$ and the symbol $\circ$ stands for convolution in time. The bath degrees of freedom can be integrated out in a standard manner. As a result, the Green function G of the LC circuit becomes dressed by its electronic environment, $G^{-1} = G_0^{-1} - \Sigma$, with a self-energy $\Sigma(t) = \sigma_z \sum_n \lambda_n^2 D_n(t)\sigma_z$.

Next, we introduce the inductive coupling between the mesoscopic device and the LC circuit, $V_{int} = \alpha q \dot{I}$, where $\dot{I}$ is the time derivative of the current operator [86]. This interaction is interpreted here as an external potential acting on the oscillator circuit. To calculate correlation functions of the LC circuit coordinate q, we introduce the generating functional,

$$\mathcal{Z}_\eta[I] = \int \mathcal{D}\mathbf{q} \exp i\Big[\frac{1}{2}\,\mathbf{q}^T \circ G^{-1} \circ \mathbf{q} - \mathbf{q}^T\sigma_z \circ (\alpha\dot{\mathbf{I}} + \eta)\Big] \ , \tag{6.3}$$

where η is a two-component auxiliary field. Performing integration over $\mathbf{q}$ results in $\mathcal{Z}_\eta[I] = e^{iS_{eff}[\eta,I]}$ with an effective action (restoring integrals):

$$S_{eff}[\eta, I] = -\frac{i}{2}\int dt \int dt' (\eta(t) + \alpha \dot{\mathbf{I}}(t))^T \sigma_z \check{G}(t-t') \sigma_z (\eta(t') + \alpha \dot{\mathbf{I}}(t')) \ . \quad (6.4)$$

The action (6.4) is then used to compute the relevant averages by taking derivatives over the auxiliary field η. As a result, one finds for the averages of fluctuating coordinate (charge) q:

$$\langle q(t) \rangle = \frac{\alpha}{2} \sum_{s=\pm} \int d\tau \sigma_z^{ss} (G^{+s}(t,\tau) + G^{-s}(t,\tau)) \ , \quad (6.5)$$

$$\begin{aligned} \delta\langle q(t) q(0) \rangle &= \alpha^2 \sum_{s_1,s_2} \sigma_z^{s_1 s_1} \sigma_z^{s_2 s_2} \\ &\times \ Z[I]^{-1} \int d\tau_1 d\tau_2 \, \langle \dot{I}(\tau_1^{s_1}) \dot{I}(\tau_2^{s_2}) Z[I] \rangle \, G^{s_1 +}(\tau_1, 0) \, G^{s_2 -}(\tau_2, t) \ , \end{aligned} \quad (6.6)$$

with $Z[I] = \mathcal{Z}_{\eta=0}[I]$, and $\langle ... \rangle$ denotes a non-equilibrium average over the mesoscopic system. Here we ignore contributions which originate from the zero-point fluctuations of the LC circuit plus bath, as these are subtracted in the excess noise and third moment measurement.

6.2 MEASURABLE NOISE AND THIRD CURRENT MOMENT

At this stage no approximation has been made on the magnitude of the inductive coupling. An expansion of the partition function in powers of α yields contributions to these averages which contain all high-order correlators of the current derivative moments. Such moments are translated into "regular" current correlators, using Fourier transforms. We start with noise, introducing the combinations $K^{\pm}(t) = \theta(t)(K^{>}(t) \pm K^{<}(t))$, where $K^{>}$ and $K^{<}$ are the off-diagonal elements of $\langle \dot{I}(t^s) \dot{I}(t'^{s'}) \rangle$ in Eq. (6.6). Going to the rotated Keldysh basis allows to rewrite the charge fluctuations at equal time as:

$$\delta\langle q^2 \rangle = \alpha^2 \int \frac{d\omega}{2\pi} G^R(\omega) \{ G^K(\omega) K^-(\omega) - (G^R(\omega) - G^A(\omega)) K^+(\omega) \} \ , \quad (6.7)$$

with the three Green function components given by

$$G^{R/A}(\omega) = [M(\omega^2 - \Omega^2) \pm i \, \mathrm{sgn}(\omega) J(|\omega|)]^{-1} \ , \quad (6.8)$$

$$G^K = (2N(\omega) + 1)(G^R(\omega) - G^A(\omega)) \ , \quad (6.9)$$

where $N(\omega)$ is the Bose occupation number of the oscillator and

$$J(\omega) = \pi \sum_n \lambda_n^2 / (2 M_n \Omega_n) \delta(\omega - \Omega_n) \quad (6.10)$$

is the bath spectral function giving rise to a finite line width for the LC circuit Green function.

The introduced time derivative correlators $K^{>,<}$ are related to the current correlators as $K^{<}(\omega) = \omega^2 S_+(\omega)$ and $K^{>}(\omega) = \omega^2 S_-(\omega)$, with

$$S_+(\omega) = \int dt \langle I(0)I(t)\rangle e^{i\omega t} \ , \quad S_-(\omega) = S_+(-\omega) \tag{6.11}$$

corresponding to the response function for emission/absorption of radiation from/to the mesoscopic circuit [86]. With these definitions, the final result for the measurable excess noise reads:

$$\delta\langle q^2\rangle = 2\alpha^2 \int_0^\infty \frac{d\omega}{2\pi}\, \omega^2 [\chi''(\omega)]^2 (S_+(\omega) + N(\omega)(S_+(\omega) - S_-(\omega))) \ , \tag{6.12}$$

where $\chi''(\omega) = J(|\omega|)/[M^2(\omega^2 - \Omega^2)^2 + J^2(|\omega|)$ is the susceptibility of [101], here generalized to arbitrary $J(|\omega|)$. Eq. (6.12) indicates that for a small line width, the integrand can be computed at the resonant frequency Ω, and the measured noise is proportional to $S_+(\Omega) + N(\Omega)(S_+(\Omega) - S_-(\Omega))$, with a prefactor which is divergent in the absence of dissipation [86]. Eq. (6.12) constitutes a mesoscopic analog of the radiation line width calculation[100]: a dissipative LC circuit cannot yield any divergences in the measurable noise. Dissipation is essential in the measurement process.

Now we turn to the measurement of the third moment. Performing a perturbative expansion in α of the average charge in Eq (6.5), only odd (time derivative) current correlators can be generated in the series. The first term is proportional to $\langle \dot{I}\rangle$, and it vanishes in a stationary situation (dc bias on the mesoscopic device). The next non-vanishing term is directly related to the third moment at finite frequencies: $L^{s_1 s_2 s_3}(t_1, t_2, t_3) = \langle T_C\{\dot{I}(t_1^{s_1})\dot{I}(t_2^{s_2})\dot{I}(t_3^{s_3})\}\rangle$ (T_C is the Kelsdysh time-ordering). The average charge is expressed in terms of the Green's functions of the LC circuit plus bath and the current correlators as:

$$\begin{aligned}\langle q(t)\rangle_{(3)} = -\frac{i}{2}\,\alpha^3 \int d\tau\, \theta(t-\tau)(G^{>}(t-\tau) - G^{<}(t-\tau)) \\ \times \int dt_1 dt_2\, \sigma_z^{s_1 s_1}\sigma_z^{s_2 s_2} G^{s_1 s_2}(t_1 - t_2) L^{+ s_1 s_2}(\tau, t_1, t_2) \ ,\end{aligned} \tag{6.13}$$

where summation over repeated Keldysh indices is assumed. It turns out that the average charge can be expressed solely in terms of a special combination of current derivative correlators:

$$R^{\pm}(\tau, t_1, t_2) \ = \ \theta(\tau - t_1)\theta(t_1 - t_2) L^{\pm}(\tau, t_1, t_2) \ , \tag{6.14}$$

with $L^{\mp}(\tau, t_1, t_2) = \langle [[\dot{I}(\tau), \dot{I}(t_1)]_-, \dot{I}(t_2)]_{\mp}\rangle$. Thus, the mesoscopic circuit correlators appear only in the form of interlocked commutators $(-)$/anti-commutators $(+)$. This is an important aspect of this scheme, because the commutator which is common for both correlators $L^{\mp}$ implies that our scheme is only effective when

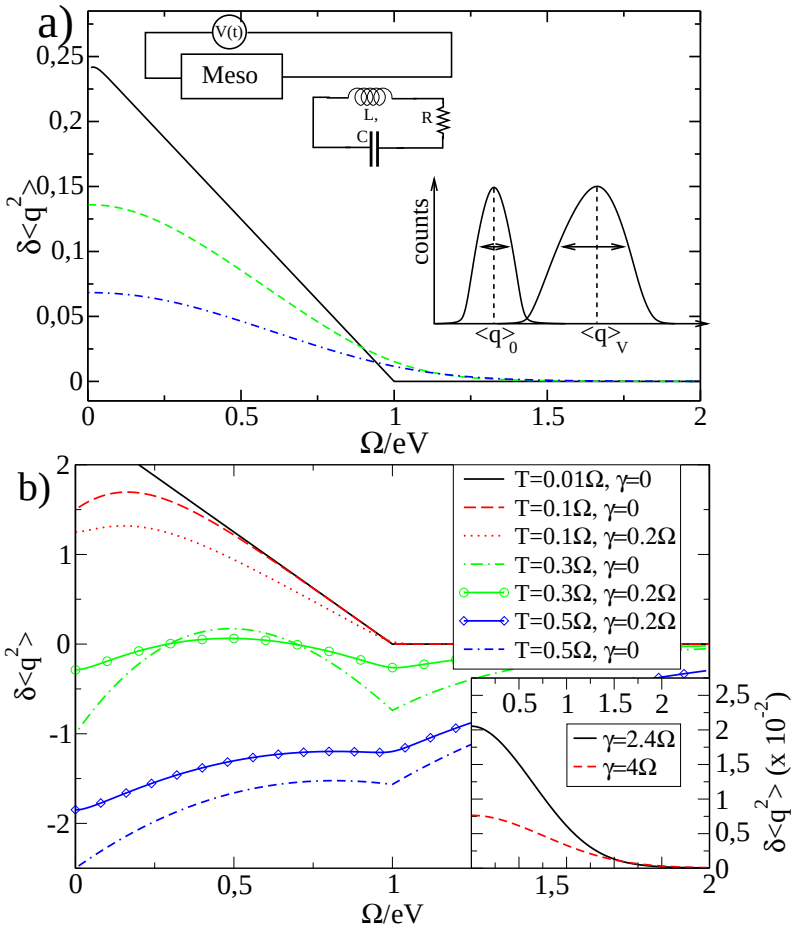

Figure 6.1: a) (top) Mesoscopic device coupled to a dissipative LC circuit. (bottom) Typical histograms of the charge used to identify the mesurable noise and the third moment, at zero and finite voltage. (main) Computed measurable noise: underdamped and low-T case, $T \ll \gamma/2 < \Omega$ ($k_B = 1$). Fixed $T = 0.01\,\Omega$ for $\gamma = 0$ (full), $\gamma = 1.6\,\Omega$ (dashed), and $\gamma = 2.4\,\Omega$ (dashed-dotted). b) Underdamped and "high"-T case, $\gamma/2 \leq T < \Omega$. Inset: overdamped and low-T case, $T \ll \Omega < \gamma/2$ ($T = 0.01\,\Omega$).

the transport is fully coherent, i.e., when the rate of escape for electrons from the mesoscopic device to the leads is large compared to the temperature. For instance, such correlators vanish in the case of incoherent Coulomb blockade transport. Exploiting time translational invariance, the final result for the measurable third moment then reads (the time dependance drops out):

$$\langle q\rangle_{(3)} = -i\alpha^3 G^R(0)\int_{-\infty}^{\infty}\frac{d\omega}{2\pi}\left[G^K(\omega)R^-(0,\omega) - (G^R(\omega)-G^A(\omega))R^+(0,\omega)\right] . \tag{6.15}$$

Note the similarity between this expression and the one obtained in Eq. (6.7) for the measurable noise: the correlators $R^{\pm}$ are weighted by the same Green function components of the LC circuit as the noise combinations $K^{\pm}$ in Eq. (6.7). Eq. (6.15) also shows which third moment correlators (and at which frequencies) the dissipative LC circuit is capable of measuring. Using the expressions of the Green function components, one obtains:

$$\langle q\rangle_{(3)} = \frac{2\alpha^3}{M\Omega^2}\int_0^{\infty} d\omega\chi''(\omega)\mathrm{Re}\Big\{(2N(\omega)+1)R^-(0,\omega) - R^+(0,\omega)\Big\} . \tag{6.16}$$

There is, however, a fundamental difference between the two responses of Eqs. (6.12) and (6.16): $\chi''(\omega)$ appears as a square in the measurable noise (6.12), while the measurable third moment (6.16) is linear in $\chi''(\omega)$. In particular, assuming a strict Ohmic or Markovian damping $J(\omega) = M\gamma\omega$ (a memoryless bath is consistent with the adiabatic switching assumption), the limit of zero dissipation, $\gamma \to 0$, does not lead to a divergence in the measurable third moment as it does in the measurable noise.

6.3 APPLICATION TO A QUANTUM POINT CONTACT

Below our results are applied to a quantum point contact (QPC). The computed measurable noise $\delta\langle q^2\rangle$ (Fig. 6.1) and third moment $\langle q\rangle_{(3)}$ (Fig. 6.2) are plotted as a function of Ω/eV (V is a bias voltage applied to the QPC) for different γ and temperature T of the LC circuit. The temperature is assumed to be small compared to the bias eV, and the QPC circuit is assumed to have a *lower* temperature than the detector. In the plots, we mostly consider the low ($k_BT < \gamma/2$) and high temperature regimes ($k_BT > \gamma/2$) in the underdamped case, $\gamma/2 < \Omega$. The overdamped regime, $\gamma/2 \geq \Omega$, is considered only for the measurable noise (inset of Fig. 1b).

In the underdamped case, the susceptibility χ'' is a superposition of Lorentzian peaks at $\pm\Omega$ and width γ. Thus, if $\gamma \ll \Omega$ we expect qualitative behavior similar to that of the undamped case, except of course that the divergence is removed. The excess noise is known to have a singular derivative at $\omega = eV$. A curve with no damping is shown (Fig. 6.1a, full line), after rescaling (it is infinite for $\gamma \to 0$). Fig. 6.1a shows that at small temperature, the effect of even weak damping is to

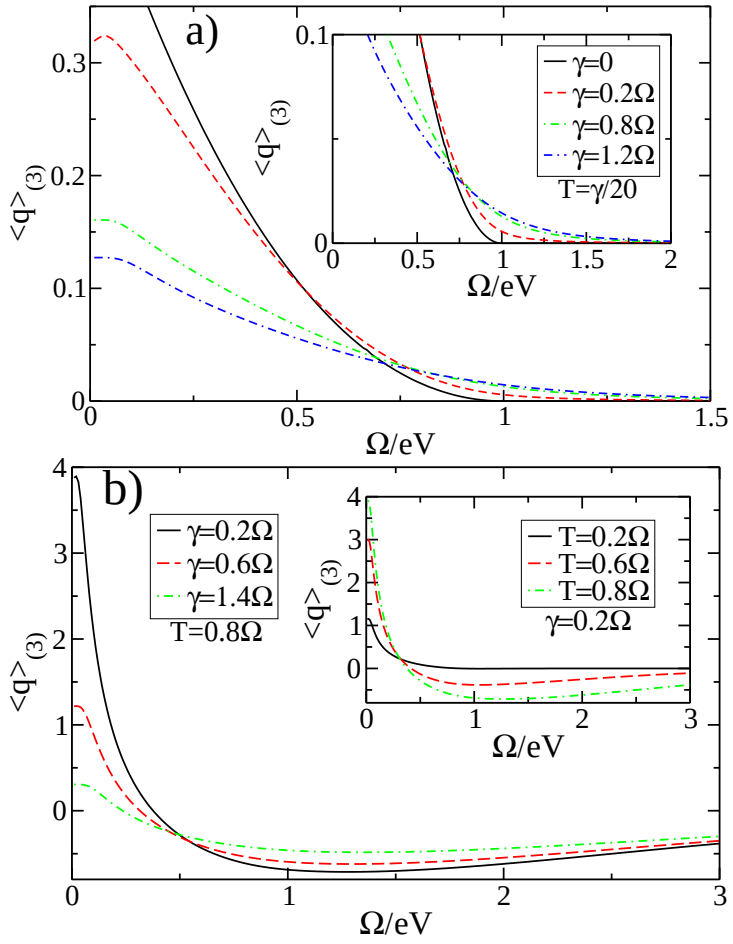

Figure 6.2: Computed measurable third moment. a) Underdamped and low-T case, $T \ll \gamma/2 < \Omega$ ($k_B = 1$), for the displayed values of the damping parameter. Inset: zoom near $\Omega = eV$. b) Underdamped and "high"-T case, $\gamma/2 < T < \Omega$ case at constant T and different values of γ. Inset: γ is fixed and T is varied.

wash out this singularity, because the coupling to the environment is equivalent to averaging over many resonant frequencies, and the measurable noise flattens out. The inset of Fig. 6.1b also applies to $k_BT < \gamma$, but deals with the overdamped regime: there is no reminiscence of the linear behavior found for weak damping because the two peaks of $\chi''(\omega)$ cannot be resolved, even at low temperatures.

Fig. 6.1b shows the effect of high temperature on the noise both without and with dissipation, in the underdamped regime. The measurable noise can become negative at higher temperature because $S_+ - S_- < 0$, and because of the increased population of LC oscillator states. As we are considering excess effects (difference between the charge fluctuations with and without the applied bias) there is no controversy here. Note that this would not be true if both the mesoscopic circuit and its detector were at the same temperature (the computed measurable noise would be positive). As in Fig. 6.1a, the cusps (or singularities), which survive for the undamped case even at these temperatures, are strongly attenuated due to damping. An important feature is that the measuring temperature T enters our results exactly as in the undamped case, because the response function $\chi''(\omega)$ is temperature-independent ($\chi''(\omega)$ is related to the symmetrized correlation function of the damped LC circuit via the fluctuation-dissipation theorem).

The computed measurable third moment (Fig. 6.2) for zero damping does not have a singularity at $\Omega = eV$, but it vanishes beyond this point, and has a linear behavior (not shown) close to $\omega = 0$. For the underdamped case $\gamma/2 < \Omega$, the main effect is to reduce its amplitude, and to wash out its vanishing at $\Omega = eV$ (see inset). One notices that it saturates near $\Omega = 0$. The effect of temperature is displayed in Fig. 6.2: the structure at $\Omega = eV$ disappears, and the width of the maximum at $\Omega = 0$ is reduced. Similarly to the measurable noise, the third moment can become negative when either damping or temperature is increased (Fig. 6.2b inset).

The above measurement setup and coupling conditions are easily achievable by on-chip inductive coupling to a SQUID circuit behaving as a harmonic oscillator. Recently reported quality factors of $\approx 100 - 150$, with an oscillator resonance of $\approx$ 3GHz, and operating temperature $T \approx 25$ mK [102, 103] correspond to the under damped regime discussed here.

CHAPTER 7

SUMMARY

In this chapter, we briefly summarize the main results obtained in papers I-IX and having been discussed in the previous chapters.

We have theoretically explored electronic transport through a single-molecular conductor connected to either normal or superconducting electrodes. The main focus has been on studying unambiguous signatures of coherent quantum behavior in the molecular junctions, on understanding the role of many-body correlation effects on the system dynamics associated with the interplay between the intrinsic degrees of freedom (vibrations, spin) of the conductor and current flow.

Considering normal electron transport through a vibrating molecule (suspended carbon nanotube), we have provided an in-depth study of negative differential conductance (NDC) behavior in this type of devices. Assuming the weak tunneling regime, so that electrons evacuated in the leads effectively loose their phase coherence (at relatively high temperature), we have used a kinetic equation formalism where the quantum mechanical nature of electron-phonon dynamics within the molecular dot (polaron formation) is taken into account yet. The positive or negative differential conductance behavior depends both on the location of the polaron level and on the occupation of the phonon sidebands captured within the bias voltage window. The NDC effect occurs when two or more phonon-assisted channels are competing in the transport, and is a hallmark of a non-equilibrium vibrational distribution on the molecule. We have clearly shown that for asymmetric tunneling rates (which corresponds to a typical experimental situation with STM measurements), there exist a wide range of parameters which lead to NDC. We have also proposed that a half-shuttle mechanism may play a role in a STM experiment, and can be detected by the asymmetry of the current-voltage curves. Although the half-shuttle mechanism tends to reinforce the negative differential regions, it cannot trigger the NDC behavior on its own.

Also, we have studied normal transport through a molecular quantum dot in the case of strong tunneling coupling to the leads (but not in the Kondo regime). Applying the non-equilibrium Green function technique in the polaron representation, we have developed a nonperturbative scheme to calculate the current–voltage characteristics of the molecule in the regime of intermediate electron-

phonon coupling. We have shown that with increasing tunneling coupling to the leads, correlations between polaron clouds become more essential at relatively high temperature, leading to strong suppression of tunnel broadening of the density of states of the molecule. The detection of such features in the molecule spectral function could be observed in the measurement of the differential conductance by varying the local temperature of the molecule (carbon nanotube). We note that the coupling to the dissipative environment of the molecule leads to an additional broadening of phonon sidebands. The possibility of phonon damping has not been included in our analysis, which could constitute an extension of our work.

In this thesis, we have also investigated how electronic transport is affected by a coherent phonon mode for the case of superconducting leads. We have computed the dc current for the full bias (V) range within a Keldysh Green function scheme valid for arbitrary phonon frequency Ω but in the weak electron-phonon coupling regime. Our main results are as follows: (i) In the subgap regime $eV < 2\Delta$, multiple Andreev reflection (MAR) processes accompanied by phonon emission cause rich structure near the onset of MAR channels, including an even-odd parity effect that can be interpreted in terms of an inelastic MAR ladder picture. Thereby we have established a connection between the Keldysh formalism and the Landauer scattering approach for inelastic MAR. (ii) For $eV \gg \Delta$, the electron-phonon interaction tends to enhance the excess current, which is defined as the difference in current for $V \to \infty$ when changing normal into superconducting leads. (iii) At equilibrium ($V = 0$), we have obtained analytical results for the Josephson current in the adiabatic limit $\hbar\Omega \ll \Delta$, which is interpreted in terms of the Andreev bound states with an effective transparency renormalized by phonons. For the future work, other quantities such as shot noise or frequency-dependent noise deserve attention. Noise can yield information about the effective charge involved in the transfer process, and how this charge is affected by phonon transitions remains to be explored.

Passing to the case of strong electron-phonon coupling, we have analyzed the Josephson transport through a molecular quantum dot with the main focus on the quantum dynamics of the local phonon mode. We have found that in the weak tunneling regime, the nonclassical phonon "cat states" (a superposition of opposite coherent states) are developed and linked to the current states associated with the Andreev bound states in the junction. These nonclassical phonon states can be "released" by performing a projective measurement of the current. For transparent lead-molecule contacts, we have shown that the Josephson effect triggers coherent phonon fluctuations and induces squeezing of the phonon mode: the conjugate momentum of the molecular distortion displays fluctuations reduced below the zero-point quantum noise level. Phonon squeezing occurs for a wide range of parameters; it is controlled by the superconducting phase difference and is maximal in the polaron crossover regime. The experimental implementation of squeezed phonons can be achieved in electronic circuits with freely suspended car-

bon nanotubes. We have proposed to use optical detection technique for probing nonclassical phonon states as a feasible way to demonstrate coherent quantum behavior in nanomechanical systems.

Another interesting possibility to observe coherent phenomena in the Josephson transport through a molecular quantum dot is realized in the junctions where the interplay between the spin degrees of freedom of the dot and bulk electrons is present. Exploring phase-coherent transport in this situation, first we have studied the Josephson current through a molecule possessing a large magnetic spin. We have shown that the coupling between the electronic spin on the dot and the (static) molecular spin can lead to the π junction behavior depending on the relative weight of partial contributions to the current from the Andreev bound states and the quasiparticle continuum. A possible extension of these studies could include decoherence and feedback effects on the molecular spin affected by a supercurrent.

Secondly, we have studied the Josephson current through a multi-level quantum dot in the presence of Rashba and Dresselhaus spin orbit couplings. For a single dot level, spin-orbit effects cancel out unless a magnetic Zeeman field is included. In this case, we have predicted spin precession (Datta-Das) effects in the Josephson current, i.e., oscillations of the critical current as a function of the effective length of the dot. These oscillations have amplitude of the order of a few tenths of the nominal critical current, which should be observable. More interestingly, for the case of a double dot, spin precession effects show up even in the absence of an external magnetic field. The supercurrent can be drastically modified, either containing sharp peaks or being largely suppressed. The experimental observation of such peaks could constitute evidence for spin-orbit effects in a superconducting transistor. Possible extensions of that work could include Coulomb interaction effects in the dot, which will be important when the tunneling rates become comparable to the dot charging energy.

Also, we have developed a theory for the Andreev level qubit, a device consisting of a SQUID with a single-channel quantum point contact (QPC), combining the features of microscopic and macroscopic quantum systems. The highly transmissive superconducting QPC may be viewed as a kind of quantum dot which contains two localized fermionic states inherently coupled to the dynamics of the superconducting phase difference (local boson mode). We have studied phonon-induced decoherence of the Andreev level qubit originating from the coupling of lead electrons with acoustic phonons in the bulk. We have shown that the fermionic nature of Andreev levels does not affect the qubit operation, but it plays an important role for the qubit decoherence: both the relaxation and dephasing processes are governed by a power law rather than an exponential one. Furthermore, we have found that the rate of phonon-induced transition between the Andreev levels is significantly reduced compared to the bulk transition rate: rapid spreading out of the Andreev level wave function in the electrodes strongly reduces the relevant phonon phase space.

Finally, in a separate study, we have considered the measurement of high frequency noise and higher current moments with a dissipative resonant circuit, which is inductively coupled to a mesoscopic device operating in the coherent regime. Information about the higher current moments is coded in the histograms of the charge on the capacitor plates of the resonant circuit. Dissipation has been included via the Caldeira-Leggett model, and it is essential for the measurable noise to remain finite. We have also identified which combinations of current correlators enter the measurement of the third moment. The latter involves the same generalized susceptibility as in the measurable noise, but it does not diverge for zero damping. The results have been illustrated for a quantum point contact.

ACKNOWLEDGEMENTS

I would like to gratefully acknowledge my great collaborator and the tutor of this thesis Thierry Martin for encouraging me to write the Habilitation thesis, for his constant support and efforts in making this thesis possible.

I would also like to thank my colleague from LPMMC Sergey Skipetrov for helping me in numerous occasions during the preparation of this thesis.

BIBLIOGRAPHY

[1] B. J. LeRoy, S. G. Lemay, J. Kong, and C. Dekker, *Electrical generation and absorbtion of phonons in carbon nanotubes*, Nature (London) **432**, 371 (2004).

[2] B. J. LeRoy, J. Kong, V. K. Pahilwani, C. Dekker, and S. G. Lemay, *Three-terminal tunneling spectroscopy of suspended carbon nanotubes*, Phys. Rev. B **72**, 075413 (2005).

[3] S. Sapmaz, P. Jarillo-Herrero, Y. M. Blanter, C. Dekker, and H. S. J. van der Zant, *Tunneling in suspended carbon nanotubes assisted by longitudinal phonons*, Phys. Rev. Lett. **96**, 026801 (2006).

[4] A. N. Pasupathy, R. C. Bialczak, J. Martinek, J. E. Grose, L. A. K. Donev, P. L. McEuen, and D. C. Ralph, *The Kondo effect in the presence of ferromagnetism*, Science **306**, 86 (2004).

[5] B. J. LeRoy, S. G. Lemay, J. Kong, and C. Dekker, *Scanning tunneling spectroscopy of suspended single-wall carbon nanotubes*, Appl. Phys. Lett. **84**, 4280 (2004).

[6] L. Y. Gorelik, A. Isacsson, M. V. Voinova, B. Kasemo, R. I. Shekhter, and M. Jonson, *Shuttle mechanism for charge transfer in Coulomb blockade nanostructures*, Phys. Rev. Lett. **80**, 4526 (1998).

[7] A. Mitra, I. Aleiner, and A. J. Millis, *Phonon effects in molecular transistors: quantal and classical treatment*, Phys. Rev. B **69**, 245302 (2004).

[8] L. Glazman and R. I. Shekhter, *Inelastic resonant tunneling of electrons through a potential barrier*, Sov. Phys. JETP **67**, 163 (1988).

[9] N. S. Wingreen, K. W. Jacobsen, and J. W. Wilkins, *Inelastic scattering in resonant tunneling*, Phys. Rev. B **40**, 11834 (1989).

[10] U. Lundin and R. H. McKenzie, *Temperature dependence of polaronic transport through single molecules and quantum dots*, Phys. Rev. B **66**, 075303 (2002).

[11] J.-X. Zhu and A. V. Balatsky, *Theory of current and shot-noise spectroscopy in single-molecular quantum dots with a phonon mode*, Phys. Rev. B **67**, 165326 (2003).

[12] A. S. Alexandrov and A. M. Bratkovsky, *Memory effect in a molecular quantum dot with strong electron-vibron interaction*, Phys. Rev. B **67**, 235312 (2003).

[13] K. Flensberg, *Tynneling broadening of vibrational sidebands in molecular transistors*, Phys. Rev. B **68**, 205323 (2003).

[14] M. Galperin, A. Nitzan, and M. A. Ratner, *Resonant inelastic tunneling in molecular junctions*, Phys. Rev. B **73**, 045314 (2006).

[15] Y. Meir and N. S. Wingreen, *Landauer formula for the current through an interacting electron region*, Phys. Rev. Lett. **68**, 2512 (1992).

[16] D. M.-T. Kuo and Y. C. Chang, *Tunneling current through a quantum dot with strong electron-phonon interaction*, Phys. Rev. B **66**, 085311 (2002).

[17] D. Feinberg, S. Ciuchi, and F. de Pasquale, *Squeezing phenomena in interacting electron-phonon systems*, Int. J. Mod. Phys. B **4**, 1317 (1990).

[18] M. R. Buitelaar, W. Belzig, T. Nussbaumer, B. Babic, C. Bruder, and C. Schönenberger, *Multiple Andreev reflections in a carbon nanotube quantum dot*, Phys. Rev. Lett. **91**, 057005 (2003).

[19] A. Y. Kasumov, R. Deblock, M. Kociak, B. Reulet, H. Bouchiat, I. I. Khodos, Y. B. Gorbatov, V. T. Volkov, C. Journet, and M. Burghard, *Supercurrents through single-walled carbon nanotubes*, Science **284**, 1508 (1999).

[20] B. Reulet, A. Y. Kasumov, M. Kociak, R. Deblock, I. I. Khodos, Y. B. G. V. T. Volkov, C. Journet, and H. Bouchiat, *Acoustoelectric effects in carbon nanotubes*, Phys. Rev. Lett. **85**, 2829 (2000).

[21] P. Jarillo-Herrero, J. A. van Dam, and L. P. Kouwenhoven, *Quantum supercurrent transistors in carbon nanotubes*, Nature (London) **439**, 953 (2006).

[22] A. Y. Kasumov, K. Tsukagoshi, M. Kawamura, T. Kobayashi, Y. Aoyagi, K. Senba, T. Kodama, H. Nishikawa, I. Ikemoto, K. Kikuchi, V. T. Volkov, Y. A. Kasumov, R. Deblock, S. Guéron, and H. Bouchiat, *Proximity effect in a superconductor-metallofullerene-superconductor molecular junction*, Phys. Rev. B **72**, 033414 (2005).

[23] T. Novotny, A. Rossini, and K. Flensberg, *Josephson current through a molecular transistor in a dissipative environment*, Phys. Rev. B **72**, 224502 (2005).

[24] T. M. Klapwijk, G. E. Blonder, and M. Tinkham, *Explanation of subharmonic energy gap structure in superconducting contacts*, Physica B+C **109-110**, 1657 (1982).

[25] E. N. Bratus', V. S. Shumeiko, and G. Wendin, *Theory of subharmonic gap structure in superconducting mesoscopic tunnel contacts*, Phys. Rev. Lett. **74**, 2110 (1995).

[26] D. Averin and A. Bardas, *ac Josephson effect in a single quantum channel*, Phys. Rev. Lett. **75**, 1831 (1995).

[27] J. C. Cuevas, A. Martin-Rodero, and A. L. Yeyati, *Hamiltonian approach to the transport properties of superconducting quantum point contacts*, Phys. Rev. B **54**, 7366 (1996).

[28] A. L. Yeyati, J. C. Cuevas, A. López-Dávalos, and A. Martin-Rodero, *Resonant tunneling through a small quantum dot coupled to superconducting leads*, Phys. Rev. B **55**, R6137 (1997).

[29] G. Johansson, E. N. Bratus', V. S. Shumeiko, and G. Wendin, *Resonant multiple Andreev reflections in mesoscopic superconducting junctions*, Phys. Rev. B **60**, 1382 (1999).

[30] S. Hershfield, J. H. Davies, and J. W. Wilkins, *Resonant tunneling through an Anderson impurity. I. Current in the symmetric model*, Phys. Rev. B **46**, 7046 (1992).

[31] A. L. Yeyati, J. C. Cuevas, and A. Martin-Rodero, *Dynamical Coulomb blockade of multiple Andreev reflections*, Phys. Rev. Lett. **95**, 056804 (2005).

[32] Z. Hang, *New type of Cooper pairing in systems with strong electron-phonon interaction*, Phys. Rev. B **37**, 7419 (1988).

[33] X. Hu and F. Nori, *Phonon squeezed states generated by second-order Raman scattering*, Phys. Rev. Lett. **79**, 4605 (1997).

[34] M. P. Blencowe and M. N. Wybourne, *Quantum squeezing of mechanical motion for micron-sized cantilevers*, Physica (Amsterdam) **280B**, 555 (2000).

[35] P. Rabl, A. Shnirman, and P. Zoller, *Generation of squeezed states of nanomechanical resonators by reservoir engineering*, Phys. Rev. B **70**, 205304 (2004).

[36] Y. D. Wang, Y. B. Gao, and C. P. Sun, *Engineering quantum decoherence of charge qubit via a nanomechanical resonator*, Eur. Phys. J. B **40**, 321 (2004).

[37] R. Ruskov, K. Schwab, and A. N. Korotkov, *Squeezing of a nanomechanical resonator by quantum nondemolition measurement and feedback*, Phys. Rev. B **71**, 235407 (2005).

[38] H. Park, J. Park, A. K. L. Lim, E. H. Andersen, A. P. Alivisatos, and P. L. McEuen, *Nanomechanical oscillations in a single-C_{60} transistor*, Nature (London) **407**, 57 (2000).

[39] A. N. Pasupathy, J. Park, C. Chang, A. V. Soldatov, S. Lebedkin, R. C. Bialczak, J. E. Grose, L. A. K. Donev, J. P. Sethna, D. C. Ralph, and P. L. McEuen, *Vibration-Assisted Electron Tunneling in C_{140} Transistors*, Nano Lett. **5**, 203 (2005).

[40] S. Sapmaz, Y. M. Blanter, L. Gurevich, and H. S. J. van der Zant, *Carbon nanotubes as nanoelectromechanical systems*, Phys. Rev. B **67**, 235414 (2003).

[41] D. F. Walls and G. J. Milburn, *Quantum Optics* (Springer, Berlin, 1994).

[42] M. S. Dresselhaus and P. C. Eklund, *Phonons in carbon nanotubes*, Adv. Phys. **49**, 705 (2000).

[43] D. Gatteschi and R. Sessoli, *Molecular nanomagnets: the first 10 years*, J. of Magnetism and Magnetic Materials **272-276**, 1030 (2005).

[44] L. N. Bulaevskii, V. V. Kuzii, and A. A. Sobyanin, *Superconductiing system with weak coupling to the current in the ground state*, JETP Lett. **25**, 290 (1977).

[45] I. Kulik, *Magnitude of the critical Josephson tunnel current*, Sov. Phys. JETP **22**, 841 (1966).

[46] A. V. Rozhkov and D. P. Arovas, *Josephson coupling through a magnetic impurity*, Phys. Rev. Lett. **82**, 2788 (1999).

[47] Z. Radovic, L. Dobrosavljevic-Grujic, and B. Vujicic, *Coexistence of stable and metastable 0 and π states in Josephson junctions*, Phys. Rev. B **63**, 214512 (2001).

[48] V. V. Ryazanov, V. A. Oboznov, A. Y. Rusanov, A. V. Veretennikov, A. A. Golubov, and J. Aarts, *Coupling of two superconductors through a ferromagnet: evidence for a π junction*, Phys. Rev. Lett. **86**, 2427 (2001).

[49] A. Buzdin and A. I. Baladie, *Theoretical description of ferromagnetic π junctions near the critical temperature*, Phys. Rev. B **67**, 184519 (2003).

[50] J. J. A. Baselmans, A. F. Morpurgo, B. J. van Wees, and T. M. Klapwijk, *Reversing the direction of the supercurrent in a controllable Josephson junction*, Nature (London) **397**, 43 (1999).

[51] A. A. Golubov, M. Y. Kupriyanov, and E. Il'ichev, *The current-phase relation in Josephson junctions*, Rev. Mod. Phys. **76**, 411 (2004).

[52] C. W. J. Beenakker, *Universal limit of critical-current fluctuations in mesoscopic Josephson junctions*, Phys. Rev. Lett. **67**, 3836 (1991).

[53] A. Krichevsky, M. Schechter, Y. Imry, and Y. Levinson, *Spectrum and thermodynamic currents in one-dimensional Josephson elements*, Phys. Rev. B **61**, 3723 (2000).

[54] T. T. Heikkila, J. Sarkka, and F. K. Wilhelm, *Supercurrent-carrying density of states in diffusive mesoscopic Josephson weak links*, Phys. Rev. B **66**, 184513 (2002).

[55] A. Levchenko, A. Kamenev, and L. I. Glazman, *Singular length dependence of critical current in SNS bridges*, cond-mat/0601177 (unpublished).

[56] Y. A. Bychkov and E. I. Rashba, *Oscillatory effects and the magnetic susceptibility of carriers in inversion layers*, J. Phys. C: Solid State Phys. **17**, 6039 (1984).

[57] S. Datta and B. Das, *Electronic analog of the electro-optic modulator*, Appl. Phys. Lett. **56**, 665 (1990).

[58] J. Nitta, T. Akazaki, H. Takayanagi, and T. Enoki, *Gate control of spin-orbit interaction in an inverted* $In_{0.53}Ga_{0.47}As/In_{0.52}Al_{0.48}As$ *heterostructure*, Phys. Rev. Lett. **78**, 1335 (1997).

[59] H. Takayanagi, T. Akazaki, and J. Nitta, *Observation of maximum supercurrent quantization in a superconducting quantum point contact*, Phys. Rev. Lett. **75**, 3533 (1995).

[60] T. Schäpers, V. A. Guzenko, R. P. Müller, A. A. Golubov, A. Brinkman, G. Crecilius, A. Kaluza, and H. Lüth, *Current-injection in a ballistic multiterminal superconductor/two-dimensional electron gas Josephson junction*, Phys. Rev. B **67**, 014522 (2003).

[61] J.-P. Cleuziou, W. Wernsdorfer, V. Bouchiat, T. Ondarçuhu, and M. Monthioux, *Carbon nanotube superconducting quantum interference device*, Nat. Nanotech. **1**, 53 (2006).

[62] Y. J. Doh, J. A. van Dam, A. L. Roest, E. P. A. M. Bakkers, L. P. Kouwenhoven, and S. D. Franceschi, *Tunable supercurrent through semiconductor nanowires*, Science **309**, 272 (2005).

[63] J. A. van Dam, Y. V. Nazarov, E. P. A. M. Bakkers, S. D. Franceschi, and L. P. Kouwenhoven, *Supercurrent reversal in quantum dots*, Nature (London) **442**, 667 (2006).

[64] K. Flensberg, *Capacitance and conductance of mesoscopic systems connected by quantum point contacts*, Phys. Rev. B **48**, 11156 (1993).

[65] K. A. Matveev, *Coulomb blockade at almost perfect transmission*, Phys. Rev. B **51**, 1743 (1995).

[66] Y. V. Nazarov, *Coulomb blockade without tunnel junctions*, Phys. Rev. Lett. **82**, 1245 (1999).

[67] E. V. Bezuglyi, A. S. Rozhavsky, I. D. Vagner, and P. Wyder, *Combined effect of Zeeman splitting and spin-orbit interaction on the Josephson current in a superconductor–two-dimensional electron gas–superconductor structure*, Phys. Rev. B **66**, 052508 (2002).

[68] J. M. Byers and M. E. Flatté, *Probing spatial correlations with nanoscale two-contact tunneling*, Phys. Rev. Lett. **74**, 306 (1995).

[69] G. Deutscher and D. Feinberg, *Coupling superconducting-ferromagnetic point contacts by Andreev reflections*, Appl. Phys. Lett. **76**, 487 (2000).

[70] O. V. Dimitrova and M. V. Feigel'man, *Two-dimensional SNS junction with Rashba spin-orbit coupling*, J. Exp. Theor. Phys. **102**, 652 (2006).

[71] Y. Makhlin, G. Schön, and A. Shnirman, *Quantum-state engineering with Josephson junction devices*, Rev. Mod. Phys. **73**, 357 (2001).

[72] G. Wendin and V. S. Shumeiko, *Superconducting quantum circuits, qubits, and computing*, cond-mat/0508729, published in Handbook of Theoretical and Computational Nanoscience, eds. M. Rieth and W. Schrommers, American Sci. Publ., 2005.

[73] C. W. Beenakker and H. V. Houten, *Josephson current through a superconducting quantum point contact shorter than the coherence length*, Phys. Rev. Lett. **66**, 3056 (1991).

[74] A. Furusaki and M. Tsukada, *Current-carrying states in Josephson junctions*, Phys. Rev. B **43**, 10164 (1991).

[75] M. C. Koops, G. V. van Duyneveldt, and R. de Bruyn Ouboter, *Direct observation of the current-phase relation of an adjustable superconducting point contact*, Phys. Rev. Lett. **77**, 2542 (1996).

[76] M. F. Goffman, R. Cron, A. L. Yeyati, P. Joyez, M. H. Devoret, D. Esteve, and C. Urbina, *Supercurrent in atomic point contacts and Andreev states*, Phys. Rev. Lett. **85**, 170 (2000).

[77] E. Scheer, P. Joyez, D. Esteve, C. Urbina, and M. H. Devoret, *Conduction channel transmissions of atomic-size aluminum contacts*, Phys. Rev. Lett. **78**, 3535 (1997).

[78] C. H. van der Wal, A. C. J. ter Haar, F. K. Wilhelm, R. N. Schouten, C. J. P. M. Harmans, T. P. Orlando, S. Lloyd, and J. E. Mooij, *Quantum superposition of macroscopic persistent-current states*, Science **290**, 773 (2000).

[79] J. R. Friedman, V. P. W. Chen, S. K. Tolpygo, and J. E. Lukens, *Quantum superposition of distinct macroscopic states*, Nature (London) **406**, 43 (2000).

[80] I. Chiorescu, Y. Nakamura, C. J. P. M. Harmans, and J. E. Mooij, *Coherent quantum dynamics of a superconducting flux qubit*, Science **299**, 1869 (2003).

[81] D. Vion, A. Aassime, A. Cottet, P. Joyez, H. Pothier, C. Urbina, D. Esteve, and M. H. Devoret, *Manipulating the quantum state of an electrical circuit*, Science **296**, 886 (2002).

[82] S. B. Kaplan, C. C. Chi, D. N. Langenberg, J. J. Chang, S. Jafarey, and D. J. Scalapino, *Quasiparticle and phonon lifetimes in superconductors*, Phys. Rev. B **14**, 4854 (1976).

[83] B. Reulet, J. Senzier, and D. E. Prober, *Environmental effects in the third moment of voltage fluctuations in a tunnel junction*, Phys. Rev. Lett. **91**, 196601 (2003).

[84] Y. Bomze, G. Gershon, D. Shovkun, L. S. Levitov, and M. Reznikov, *Measurement of counting statistics of electron transport in a tunnel junction*, Phys. Rev. Lett. **95**, 176601 (2005).

[85] S. Gustavsson, R. Leturcq, B. Simovic, R. Schleser, T. Ihn, P. Studerus, K. Ensslin, D. C. Driscoll, and A. C. Gossard, *Counting statistics of single electron transport in a quantum dot*, Phys. Rev. Lett. **96**, 076605 (2006).

[86] G. B. Lesovik and R. Loosen, *On the detection of finite-frequency current fluctuations*, JETP Lett. **65**, 295 (1997).

[87] U. Gavish, I. Imry, and Y. Levinson, *Detection of quantum noise*, PRB **62**, 10637 (2000).

[88] R. Aguado and L. P. Kouwenhoven, *Double quantum dots as detectors of high-frequency quantum noise in mesoscopic conductors*, Phys. Rev. Lett. **84**, 1986 (2000).

[89] E. Onac, F. Balestro, B. Trauzettel, C. F. J. Lodewijk, and L. P. Kouwenhoven, *Shot-noise detection in a carbon nanotube quantum dot*, Phys. Rev. Lett. **96**, 026803 (2006).

[90] R. Deblock, E. Onac, L. Gurevich, and L. P. Kouvenhoven, *Detection of quantum noise from an electrically driven two-level system*, Science **301**, 203 (2003).

[91] P.-M. Billangeon, F. Pierre, H. Bouchiat, and R. Deblock, *Emission and absorption asymmetry in the quantum noise of a Josephson junction*, Phys. Rev. Lett. **96**, 136804 (2006).

[92] B. Trauzettel, I. Safi, F. Dolcini, and H. Grabert, *Appearance of fractional charge in the noise of nonchiral Luttinger liquids*, Phys. Rev. Lett. **92**, 226405 (2004).

[93] A. V. Lebedev, A. Crépieux, and T. Martin, *Electron injection in a nanotube with leads: finite-frequency noise correlations and anomalous charges*, PRB **71**, 075416 (2005).

[94] C. W. J. Beenakker, M. Kindermann, and Y. V. Nazarov, *Temperature-dependent third cumulant of tunneling noise*, Phys. Rev. Lett. **90**, 176802 (2003).

[95] J. Tobiska and Y. V. Nazarov, *Josephson Junctions as threshold detectors for Full Counting Statistics*, Phys. Rev. Lett. **93**, 106801 (2004).

[96] J. P. Pekola, *Josephson Junction as a detector of Poissonian charge injection*, Phys. Rev. Lett. **93**, 206601 (2006).

[97] T. T. Heikkilä, P. Virtanen, G. Johansson, and F. K. Wilhelm, *Measuring non-Gaussian fluctuations through incoherent Cooper-pair current*, Phys. Rev. Lett. **93**, 247005 (2004).

[98] V. Brosco, R. Fazio, F. W. J. Hekking, and J. P. Pekola, *Model of qubits as devices to detect the third moment of current fluctuations*, PRB **74**, 024524 (2006).

[99] J. Gabelli, L.-H. Reydellet, G. Feve, J.-M. Berroir, B. Plaçais, P. Roche, and D. C. Glattli, *Hanbury Brown–Twiss correlations to probe the population statistics of GHz photons emitted by conductors*, Phys. Rev. Lett. **93**, 056801 (2004).

[100] A. I. Larkin and Y. N. Ovchinnikov, *Radiation line width in the Josephson effect*, Sov. Phys. JETP **26**, 1219 (1968).

[101] A. O. Caldeira and A. J. Leggett, *Path integral approach to quantum Brownian motion*, Physica (Amsterdam) **121A**, 587 (1983).

[102] I. Chiorescu, P. Bertet, K. Semba, Y. Nakamura, C. J. P. M. Harmans, and J. E. Mooij, *Coherent dynamics of a flux qubit coupled to a harmonic oscillator*, Nature (London) **431**, 159 (2004).

[103] J. Johansson, S. Saito, T. Meno, H. Nakano, M. Ueda, K. Semba, and H. Takayanagi, *Vacuum Rabi oscillations in a macroscopic superconducting qubit LC oscillator system*, Phys. Rev. Lett. **96**, 127006 (2006).

Curriculum Vitae

Curriculum Vitae

July 2007

Name:	Oleksandr Zazunov
Citizenship:	Ukraine
Date of birth:	June 10, 1968
Marital status:	Single
Address:	LPMMC – Maison des Magistères 25, Av. des Martyrs, BP 166 38042 Grenoble, France
Phone:	33 (0)4 76 88 79 82
Fax:	33 (0)4 76 88 79 83
E-mail:	alex.zazunov@grenoble.cnrs.fr

Present position

January 2006 - December 2007

Post-doctoral fellow within the EU project EuroSQIP (European Superconducting Quantum Information Processor),
Laboratoire de Physique et Modélisation des Milieux Condensés,
Université Joseph Fourier et CNRS, Grenoble

Post-docs

January 2005 - December 2005

Post-doctoral fellow at LEPES CNRS, Grenoble
and Centre de Physique Théorique, Marseille

January 2003 - December 2004

Post-doctoral fellow in the group of Applied Quantum Physics at Chalmers University of Technology, Göteborg, Sweden

Education

November 2000 - December 2002
Ph.D. in Physics at the Dept. of Microelectronics and Nanoscience at Chalmers University of Technology, Göteborg, Sweden

Doctoral Thesis: "Collective Electron Dynamics in Mesoscopic System"
Supervisor: Prof. Vitaly Shumeiko

March 1995 - April 1998

Postgraduate studies at Institute of Monocristals at Academy of Science of Ukraine, Kharkov, Ukraine

September 1990 - February 1995

Master of Science in Theoretical Physics (the highest honor) at the Dept. of Physics and Technology at the Kharkov State University, Ukraine

Master Thesis: "Resonant Josephson current through a single localized state in the tunnel barrier"
Supervisor: Dr. Victor Khlus

September 1985 - August 1989

Undergraduate studies for engineer's degree at the Dept. of Radio Engineering and Cybernetics at Moscow Institute of Physics and Technology, Russia.
After these studies I changed my career to theoretical physics.

Appointments

May 2000 - October 2000

Project researcher at the Dept. of Physical Chemistry at the Kharkov State Polytechnic University, Ukraine

May 1998 - April 2000

Contract computer programmer at Kharkov State Polytechnic University

September 1989 - August 1990

Laboratory assistant at the Dept. of Physical Chemistry at Kharkov Polytechnic Institute

Research skills

Quantum field theory methods. Path integral technique. Keldysh Green function formalism. Scattering theory. Programming languages C, C++.

Research experience

Strongly correlated electron systems. Collective phenomena in FQHE. Macroscopic quantum

phenomena in superconducting circuits. Quantum information. Superconducting transport in complex mesoscopic structures. Strong electron-phonon interacting systems.

Teaching experience

During my post-doc at Chalmers University in 2003-2004 I co-supervised PhD students Jonn Lantz and Margareta Wallquist sharing with them my knowledge of the theory of superconductivity and of dissipative quantum systems. At the same time, I took the post-graduate course "Pedagogics and presentation" given at Chalmers.

During my post-doc at CPT in Marseille in 2005 I was tutoring PhD student Marjorie Creux and post-doc Colin Benjamin, and later, in 2006, PhD student Alexandre Popoff. Being experienced in using the methods of quantum field theory, I taught them the principles of path-integral approach and its applications in condensed matter physics.

Since 2006 and until now, at LPMMC in Grenoble I have been tutoring PhD student Nicolas Didier in using the methods of Keldysh technique.

List of publications

1. *Resonant tunneling through a single localized state in a normal metal - superconductor junction*, V. A. Khlus, A. V. Dyomin, and A. L. Zazunov, Physica C **214**, 413 (1993).
2. *Light scattering by acoustic phonons coupled to a two-dimensional collective anyon mode*, D. V. Fil and A. L. Zazunov, Low Temp. Phys. **22**, 1095 (1996).
3. *Neutron scattering and diffusive X-ray diffraction in acoustic modes in* Nd_2CuO_4, D. V. Fil and A. L. Zazunov, Low Temp. Phys. **23**, 665 (1997).
4. *Brillouin light scattering, X-ray diffraction and neutron scattering spectroscopy of collective soundlike plane mode in HTSC cuprates*, D. V. Fil and A. L. Zazunov, Physica C **282-287**, 1045 (1997).
5. *Oscillations of the spectrum of acoustic phonons interacting with composite fermions*, A. L. Zazunov and D. V. Fil, Low Temp. Phys. **23**, 1010 (1997).
6. *Zones of absolute accumulation and elimination of radiation defects*, V. M. Koshkin, A. L. Zazunov and V. D. Ryzhikov, Journal of Funct. Mat. **6**, 53 (2000).
7. *Defect interaction and radiation properties of multicomponent semiconductors*, V. M. Koshkin, A. L. Zazunov, V. D. Ryzhikov and L. P. Galchinetsky, Journal of Funct. Mat. **8**, 240 (2001).
8. *Andreev level qubit*, A. Zazunov, V. S. Shumeiko, E. N. Bratus', J. Lantz, and G. Wendin, Phys. Rev. Lett. **90**, 087003 (2003).
9. *Dynamics and phonon-induced decoherence of Andreev level qubit*, A. Zazunov, V. S. Shumeiko, G. Wendin, and E. N. Bratus', Phys. Rev. B **71**, 214505 (2005).
10. *Phonon-mediated negative differential conductance in molecular quantum dots*, A. Zazunov, D. Feinberg, and T. Martin, Phys. Rev. B **73**, 115405 (2006).
11. *Phonon squeezing in a superconducting molecular transistor*, A. Zazunov, D. Feinberg, and T. Martin, Phys. Rev. Lett. **97**, 196801 (2006).
12. *Superconducting transport through a vibrating molecule*, A. Zazunov, R. Egger, C. Mora, and T. Martin, Phys. Rev. B **73**, 214501 (2006).
13. *Josephson current through a magnetic molecule: pi junction behavior*, T. Jonckheere, A. Zazunov, C. Benjamin, and T. Martin, in Proc. of the 6th Rencontres du Vietnam, editor J. Tran Thanh Van (Hanoi, 2006).
14. *Josephson current through a quantum dot with spin-orbit coupling*, L. Dell'Anna, A. Zazunov, R. Egger, and T. Martin, Phys. Rev. B **75**, 085305 (2007).
15. *Measuring noise and cross correlations at high frequencies in nanophysics*, M. Creux, A. Zazunov, T.K.T. Nguyen, A. Crépieux, and T. Martin, Proc. of International Symposium on Mesoscopic Superconductivity and Spintronics (MS+S2006), NTT BRL, Atsugi, Japan (World Scientific, 2007).
16. *Controllable* π *junction in a Josephson quantum-dot device with molecular spin*, C. Benjamin, T. Jonckheere, A. Zazunov, and T. Martin, Eur. Phys. J. B **57**, 279 (2007).
17. *Transport through a molecular quantum dot in the polaron crossover regime*, A. Zazunov and T. Martin, cond-mat/0703626, to appear in Phys. Rev. B (2007).
18. *Detection of finite frequency current moments with a dissipative resonant circuit*, A. Zazunov, M. Creux, E. Paladino, A. Crépieux, and T. Martin, cond-mat/0702247, to appear in Phys. Rev. Lett. (2007).

Recently submitted papers

1. *Charge skipping in a metallic grain capacitively coupled to a superconducting island*, C. Holmqvist, D. Feinberg, and A. Zazunov, cond-mat/0703412 (submitted to Phys. Rev. Lett.)
2. *Charge diffusion and duality in Josephson junctions and superconducting nanowires*, A. Zazunov, N. Didier, and F. W. J. Hekking, cond-mat/07062260 (submitted to Phys. Rev. Lett.)
3. *Rabi-like oscillations of an anharmonic oscillator: classical or quantum effect?*, J. Claudon, A. Zazunov, F. W. J. Hekking, and O. Buisson (submitted to Phys. Rev. Lett.)